CellPress

Matter

Review

Band Engineering of Carbon Nanotubes for Device Applications

Liu Qian,[1] Ying Xie,[1] Shuchen Zhang,[1] and Jin Zhang[1,*]

Carbon nanotubes (CNTs)—especially single-walled CNTs—are promising for device applications. Although CNTs have excellent intrinsic properties, their diverse band structures bring difficulties to improving the performances of CNT-based devices. Therefore, band engineering is necessary. For diverse electrical properties, selective enrichment of CNTs with specific electrical properties is essential for determining their corresponding application fields. For a certain band structure, methods such as doping can be used to slightly tune the energy bands of CNTs and make them more suitable for specific devices. Additionally, for some intrinsic limitations, construction of heterostructures with other functional materials is an effective way to tune the carrier transport at the interface and broaden the application range of CNTs. In this review, we discuss in detail the band engineering of CNTs and corresponding device applications from the respect of both microscopic and macroscopic devices. We present an outlook that controlled synthesis will determine the future applications and proper manufacture will improve the application qualities.

INTRODUCTION

Carbon nanotubes (CNTs) have long been considered as promising materials for next-generation electronic systems because of their excellent electrical, optical, and mechanical properties.[1,2] As one-dimensional (1D) nanomaterials, CNTs have unique and diverse band structures, making them suitable for various devices. Single-walled CNTs (SWNTs) have high carrier mobilities, ballistic transport, and excellent stability, which are advantageous for nanoelectronics and integrated circuits (ICs).[3] Owing to their direct-band-gap structure and excellent optical and thermal properties, CNTs are also frequently investigated in optoelectronics and thermoelectricity. Additionally, the processability of CNT products allows them to be applied in different devices with different morphologies, such as individual tubes, CNT fibers, and films. In 2019, RV16X-NANO—a microprocessor composed of more than 14,000 complementary metal-oxide semiconductor (CMOS) transistors—was developed,[4] representing a new step in the device application of CNTs.

However, in practical devices, diverse band structures of CNTs make it difficult to improve their performances. For example, in CNT field-effect transistors (FETs), the presence of metallic CNTs can lead to device failure. Therefore, purifying, modulating, or designing the CNT band structures to satisfy specific application requirements is crucial for promoting the development of CNT-based devices. For the diverse electrical properties of CNTs, the enrichment of specific electrical properties is essential because it determines the corresponding application fields, such as semiconducting tubes for FETs[5] and metallic tubes for interconnects.[2] For given band structures of CNTs, methods such as doping can be used to tune the energy

Progress and potential

Since the discovery of carbon nanotubes (CNTs) in 1991, research has been performed on their synthesis and applications. Among all the applications, electrical devices are the most promising because of their unique band structures. Nearly all breakthroughs related to devices are accompanied by improvements in the synthesis and processing of CNTs. Therefore, for further applications, the development of CNT-based material processing and device applications should be specially focused upon. With regard to electrical devices, the processing of materials is mainly referred to as band engineering of CNTs, which includes the selective enrichment of CNTs with specific electrical properties, the modulation of energy bands, and the construction of heterostructures. Devices based on CNTs and their aggregates are steadily advancing, and future efforts should be focused on material synthesis and device manufacture together with proper band engineering.

bands, making them suitable for specific devices such as n-doped CNTs for n-type FETs.[6] Additionally, addressing some of the intrinsic limitations of CNTs, construction of heterostructures with other functional materials is an effective way to tune the carrier transport at the interface and broaden the application of CNTs, such as CNT-Si heterostructures for solar cells.[7] Here, we propose the band engineering of CNTs, which significantly affects the performance of CNT-based devices. We also review the main electrical applications of CNTs and their aggregates in terms of both materials and devices. Applications in microscopic and macroscopic scales are discussed respectively because devices with different sizes have different requirements for materials. Finally, we discuss the development and design of CNT-based synthesis and manufacturing.

BAND ENGINEERING OF CNTs

In the semiconductor industry, the process of optimizing the electrical and optical properties of semiconductor materials via doping, solid solutions, and the construction of heterostructures is called band engineering. We extend the concept of band engineering to CNTs, and all the approaches for optimizing the band structures of CNTs to improve the device performance are referred to as CNT band engineering. In this section, we introduce the basic physics of CNT band structures and then introduce band engineering, including the selective enrichment of CNTs with specific electrical properties, modulation of energy bands, and construction of heterostructures based on CNTs.

Band Structures and Electrical Properties of CNTs

The understanding of the band structures of CNTs should start from their atomic structures. An individual SWNT can be structurally regarded as a hollow cylinder rolled up from a graphene sheet. As shown in Figure 1A, the structure of an SWNT can be specifically represented by a vector $\mathbf{C}$, which indicates the direction and length of the rolling up and is called the chiral vector. The chiral vector can be obtained from the basis vectors of the graphene sheet $\mathbf{a}_1$ and $\mathbf{a}_2$ as $\mathbf{C} = n\mathbf{a}_1 + m\mathbf{a}_2$, and this SWNT can be labeled according to its chiral index as (n, m) (n and m are integers, and $n \geq m$). A given SWNT can also be specified by its chiral angle θ and diameter d, where θ is defined by the angle between $\mathbf{C}$ and $\mathbf{a}_1$. The structural parameters for an SWNT can thus be obtained as follows:[8,9]

$$|\boldsymbol{a}_1| = |\boldsymbol{a}_2| = \sqrt{3}a_{cc} = 0.246\ nm \quad (a_{cc} \text{ is the C} - \text{C bond length}),$$

$$|\mathbf{C}| = 0.246\sqrt{n^2 + nm + m^2},$$

$$d = \frac{0.246}{\pi}\sqrt{n^2 + nm + m^2},$$

$$\theta = \tan^{-1}\left(\frac{\sqrt{3}\,m}{2n + m}\right).$$

Figure 1B shows three typical SWNT structures: zigzag tubes ($m = 0$, $\theta = 0$), armchair tubes ($n = m$, $\theta = 30°$), and chiral tubes ($n \neq m$, $0 < |\theta| < 30°$). The atomic structures of SWNTs have been directly observed via high-resolution transmission electron microscopy (TEM) and scanning tunneling microscopy (STM) (Figures 1C and 1D).[10,11]

The chiral indices (n, m) reflect the geometric structures and determine the metallic or semiconducting behaviors of SWNTs. The band structure of SWNTs can be derived from that of graphene. According to the zone-folding approximation, the

[1]Center for Nanochemistry, Beijing Science and Engineering Center for Nanocarbons, Beijing National Laboratory for Molecular Sciences, College of Chemistry and Molecular Engineering, Peking University, Beijing 100871, P.R. China

*Correspondence: jinzhang@pku.edu.cn

https://doi.org/10.1016/j.matt.2020.06.014

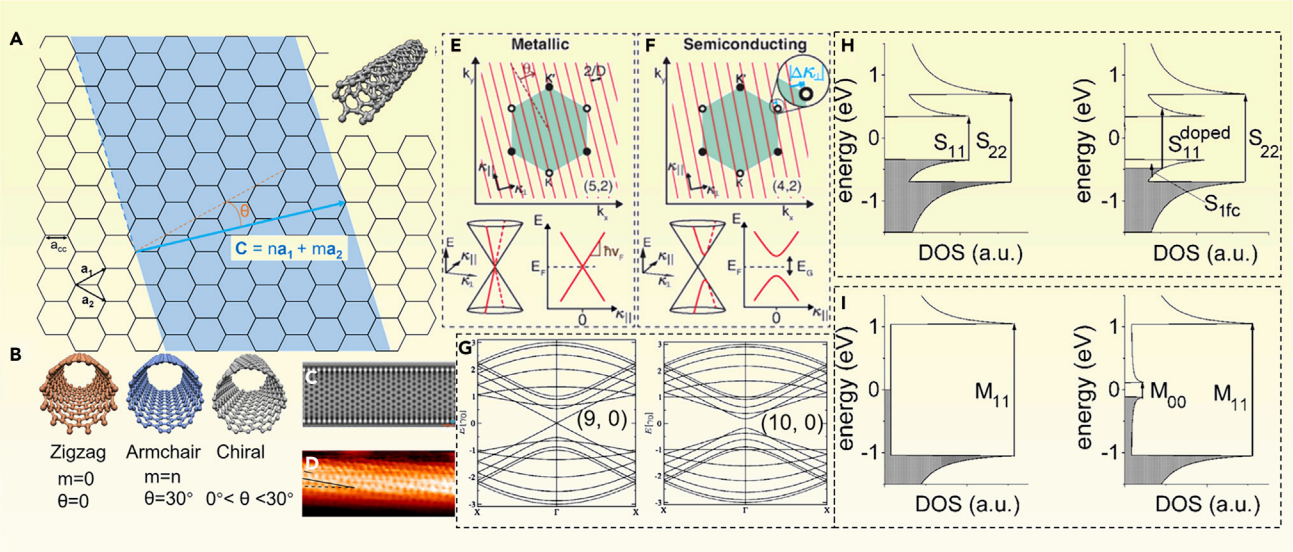

Figure 1. Atomic Structure and Band Structures of CNTs

(A) Derivation of the SWNT structure from graphene.

(B) Three typical SWNT structures according to their chiral angle θ.

(C and D) CNTs directly observed via TEM and STM. (C) TEM (a (28, 0) zigzag nanotube); Adapted with permission from Warner et al.[10] Copyright 2011, Springer Nature. (D) STM. Adapted with permission from Venema et al.[11] Copyright 1998, Springer Nature.

(E and F) Derivation of CNTs with different electrical properties.[9] If quantization lines pass through the Dirac points, the nanotube is (E) metallic; otherwise, it is (F) semiconducting. Adapted with permission from Laird et al.[9] Copyright 2015, American Physical Society.

(G–I) (G) Band structures for a (9, 0) and a (10, 0) zigzag tube based on the zone-folding model. Adapted with permission from Charlier et al.[8] Copyright 2007, American Physical Society. The Fermi level is located at zero energy. Schematic showing the density of states (DOS): (H) semiconducting tubes (left) and under hole-doped conditions (right); (I) metallic tubes (left) and with a small band gap (right). Adapted with permission from Itkis et al.[12] Copyright 2002, American Chemical Society.

band structure of graphene is approximately unperturbed after rolling up, except for the introduction of a periodic boundary condition.[13,14] This quantized boundary condition is expressed as $\mathbf{k} \cdot \mathbf{C} = 2\pi p$, where p is an integer. The perpendicular component of $\mathbf{k}$ to the tube axis is $k_c = 2p/d$.[9] Thus, in the reciprocal space, only a series of parallel quantization lines with a space of $2/d$ are allowed in the Brillouin zone of graphene. The band structure of a specific SWNT can be obtained along these cutting lines, whose orientation, length, and number depend on the chiral index of the SWNT.[8] The band gap of the SWNT depends on the minimum distance of the quantization lines from the Dirac points.[9] According to the aforementioned simple scheme, if one of the quantization lines passes straight through the Dirac points of the graphene (Figure 1E), the SWNT has a zero band gap and is metallic. Otherwise (Figure 1F), the dispersion relation exhibits a pair of hyperbolas with a band gap, and it is a semiconducting tube. A simple rule for determining the electrical property is as follows: if $(n - m)/3$ is an integer, the tubes are metallic; otherwise, they are semiconducting, with a band gap.[13–15] Experimentally, "narrow-gap" behavior is more common than metallic behavior, and yields a small band gap ($E_g \approx k_B T$) at room temperature.[16] This is due to the perturbations of the symmetry of the carbon bonds outside of the "zone-folding approximation." The perturbations may be curvature or strain.[17]

The calculated 1D dispersion relations of two typical tubes are presented in Figure 1G, showing a metallic (9, 0) tube with the Fermi surface located at Γ and a semiconducting (10, 0) tube with a band gap at Γ.[8] Figures 1H and 1I present typical schematics of the density of states (DOS) of semiconducting and metallic SWNTs,

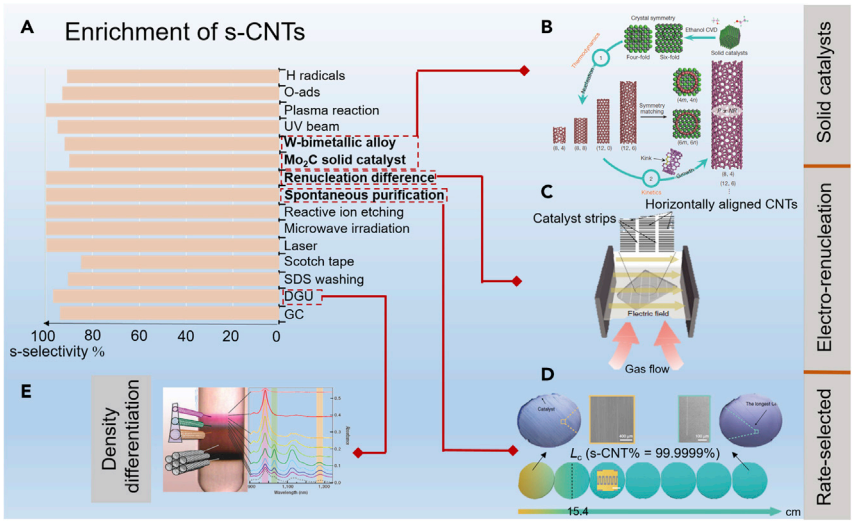

Figure 2. Typical Methods for the Selective Enrichment of Semiconducting Tubes

(A) Chart of the enrichment methods and the corresponding semiconducting selectivity.

(B) Direct growth method based on the thermodynamically and kinetically controlled CVD process. Adapted with permission from Zhang et al.[21] Copyright 2017, Springer Nature.

(C) ERN approach. Adapted with permission from Wang et al.[22] Copyright 2018, Springer Nature.

(D) Rate-selected growth method. Adapted with permission from Zhu et al.[23] Copyright 2019, Springer Nature.

(E) DGU solution separation method. Adapted with permission from Arnold et al.[24] Copyright 2006, Springer Nature.

showing Van Hove singularities[18] and electronic transitions between them. In semiconducting SWNTs, S_{11} and S_{22} correspond to the first and second interband transitions, respectively. For a hole-doped semiconducting SWNT, the introduction of an S_{11}-doped energy level may result in intraband transitions involving free carriers (S_{1fc}) and may contribute to the far-infrared absorption. For a metallic SWNT, M_{11} is the first interband transition, and M_{00} is derived from the aforementioned "narrow-gap" behavior or the pseudogap phenomenon,[19,20] which may also contribute to the far-infrared absorption.[12] Further modulation of the energy bands will be discussed later in this paper.

According to the foregoing, SWNTs have different band structures according to their atomic structures and local environment, resulting in various electrical properties. In practical applications, uniform band structures and specific electrical properties are usually beneficial to the device performance, which points to the importance of CNT band engineering.

Selective Enrichment of CNTs with Specific Electrical Properties

One of the most intriguing properties of CNTs is that their electronic structure is closely related to their geometric structure. As mentioned above, under normal conditions approximately one-third of CNTs are metallic and two-thirds are semiconducting. However, a uniform electronic type of CNTs is needed to achieve high performance of certain electrical devices. There are two main ways to increase the electronic purity of CNTs: the direct growth methods and post-treatment. Figure 2A presents typical methods for selectively enriching semiconducting tubes and corresponding purities.

Direct Growth Methods

Direct growth methods include controlled growth and selective etching during growth. Controlled growth, which is mainly based on catalyst design and growth condition design,[25,26] highly depends on the intrinsic property differences of chiral structures or band structures. Zhang et al. realized the enrichment of metallic (12, 6) tubes and semiconducting (8, 4) tubes using solid Mo_2C and WC catalysts, respectively, by thermodynamically and kinetically controlled chemical vapor deposition (CVD) growth (Figure 2B).[21] They further designed a near-equilibrium nucleation process and enriched a new family of (n, $n - 1$) semiconducting SWNTs.[27] Wang et al. claimed that when an electric field is introduced as a perturbation, metallic CNTs (m-CNTs) may be twisted into semiconducting CNTs (s-CNTs) owing to the electronic DOS-difference-caused "renucleation barrier difference" between m-CNTs and s-CNTs. This electro-renucleation (ERN) approach led to nearly defect-free s-CNT arrays with <0.1% residual m-CNTs (Figure 2C).[22] Moreover, Zhu et al. reported the spontaneous purification of CNTs with 99.9999% s-CNTs when the lengths were over 154 mm.[23] These rate-selected s-CNT arrays were based on strong interlocking between the atomic assembly rate and the band-gap structure of the CNTs, which resulted in nearly 10-fold faster decay rate of the m-CNTs than s-CNTs (Figure 2D).

On the other hand, differences in the chemical reactivity of s-CNTs and m-CNTs are always considered for selectively etching specific CNTs that react more actively with the introduced reagents or applied field. m-CNTs tend to be more reactive than s-CNTs with similar diameters owing to their different ionization energies. Oxidation by etchants[28] or perturbation via an external field[29,30] with high energy (e.g., plasma, UV light, microwave) have been proposed to enrich s-CNTs *in situ*. Nevertheless, a tradeoff must be made between the semiconducting selectivity and the array density because one-third of the CNTs are removed. The weak oxidative effect during CNT synthesis yields a relatively low selectivity, as there is little difference between the two types of CNTs during nucleation and growth in CVD. Direct growth methods have considerable application potential because of the much easier preparation process without the introduction of impurities. However, achieving a high purity and large-scale synthesis remain challenging.

Post-treatment

In addition to etching during the growth process, post-growth separation, such as *ex situ* removal, is also a desirable way to purify CNTs, e.g., selective reactions or selective wrapping. Owing to their higher conductivity compared with s-CNTs, m-CNTs can produce more Joule heat (induced by large currents). Jin et al. used this mechanism to enrich polymer-coated s-CNTs while exposed m-CNTs were removed by reactive-ion etching.[31] Other methods that initiate thermocapillary flows and selectively heat m-CNTs using microwave radiation[32] or infrared laser irradiation[33] can be adopted to achieve similar results. Selective wrapping for purifying CNTs involves noncovalent selective interactions between CNTs and other molecules. For instance, a polydimethylsiloxane-based smart Scotch tape[34] can be used to extract s-CNTs or m-CNTs from the array mixtures, and washing off m-CNTs using sodium dodecyl sulfate[35] has proved to be a facile method for separation. However, the final array density for *ex situ* selective etching or wrapping depends on the density of the original arrays, limiting the applicability of these methods.

Among all the post-treatment methods, solution-phase separation exhibits the best reproducibility and yield. Density gradient ultracentrifugation (DGU) (Figure 2E)[24] and gel chromatography[36] are the most widely used methods. The key factors in these

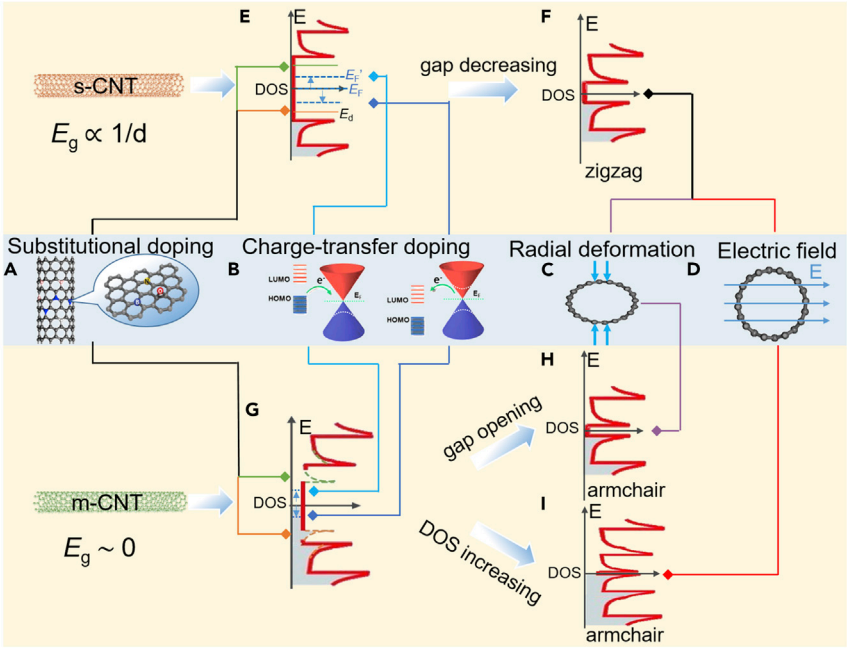

Figure 3. Modulation of Band Structures

(A–D) Typical methods for tuning the energy band of CNTs: ([A] and [B]) doping,[40] (C) radial deformation, and (D) introducing an electrical field. Adapted with permission from Maiti et al.[40] Copyright 2013, John Wiley and Sons.

(E–I) Corresponding changes in the band structures for semiconducting CNTs (s-CNT; [E] and [F]) and metallic CNTs (m-CNT; [G]–[I]).

methods are the density gradient medium and the adopted surfactants. Both of these techniques can provide a high selectivity, even a single chirality, with appropriate surfactants. However, the high technical threshold and complexity limit their applicability. Aqueous two-phase extraction,[37] which has low cost, high yield, and high concentration, can be realized within a short separation time but is restricted by the difficulty of strict control of the polymerization degree. Regarding selective dispersion,[38] although the separation purity is high, the biomolecules and conjugated polymers are expensive. However, CNTs purified via the aforementioned post-treatments have common drawbacks: they are short in length, have intrinsic structural defects, and require subsequent purification, e.g., sonication; this may induce further damage and overlap to the tubes, which is detrimental to electrical devices.

So far, neither the direct growth method nor post-treatment have been ideal for achieving the ultimate goals of 99.9999% semiconducting selectivity and a high density of >125 nanotubes/μm in a horizontal array.[39] More efforts are needed to make a breakthrough. Moreover, the enrichment of CNTs with specific electrical properties determines their applicability in different fields, but for a specific function in a certain device, the design of band structures and band alignment with other materials are still necessary to improve the device performance.

Modulation of Energy Bands

In practical devices, specific band structures, such as p-type or n-type semiconductors, closing a band gap in semiconducting CNTs or opening a band gap in metallic CNTs, are usually needed to satisfy specific device requirements. Under ambient conditions, CNTs are p-doped as a result of the physisorption of oxygen molecules on their surfaces. In this section, the reported methods (Figures 3A–3D) for tuning

the energy bands of CNTs are discussed from theoretical and experimental viewpoints.

Doping

There are two main categories of doping for CNTs: substitutional doping of heteroatoms in the CNT lattice (Figure 3A) and charge-transfer doping (Figure 3B).[40] To realize heteroatom substitution, doped CNTs can be obtained by *in situ* introduction of foreign atoms in the vapor or through solid sources during traditional synthesis methods of CNTs, such as NH_3, B_2H_6, thiophene/sulfur powder, and triphenylphosphine for N-, B-, S-, and P-doping, respectively. Post-synthetic doping tends to be difficult because of the chemical inertness of CNTs. Therefore, more-reactive oxidized CNTs are frequently employed as the starting material and annealed in the presence of proper doping species.

Dopant atoms can create impurity states in the band structure of CNTs and ultimately influence the overall electronic band configuration. The most typical types of doping are N- and B-doping. N-dopants have three possible configurations: quaternary, pyridinic, and pyrrolic. For semiconducting SWNTs, N-doping with a quaternary configuration incorporates localized states into the band gap near the bottom of the conduction band (Figure 3E). Because of the complex hybridization between the impurity state and the existing unoccupied bands, the Fermi level is raised, approaching the conduction band; this endows the CNTs with metallic behavior. For example, STM and scanning tunneling spectroscopy (STS) studies revealed that N-doped multiwalled CNTs (MWNTs) are metallic and exhibit prominent donor peaks above the Fermi energy at approximately 0.18 eV.[41] For metallic SWNTs, the impurity state generated by N-doping resides in the conduction band (Figure 3G).[42] Pyridinic N-doping leads to either p- or n-type doping, depending on the doping level (p-type is more common). If N-doping adopts a pyrrolic configuration, the five-membered ring structure may lead to a positive curvature, promoting tube closure. For B-doping, all three valence electrons of the B atom participate in σ bonding with neighboring C atoms.[43] The absence of additional electrons for original Π bonding leads to a p-doping effect. Carroll et al. detected new peaks in the valence band of MWNTs after B-doping using STS.[44] They suggested that rather than isolated substitutional B atoms, the dopant-rich BC_3 islands might significantly alter the local DOS from a semimetal to an intrinsic metal.

Charge-transfer doping relies on spontaneous charge transfer from physisorbed species, shifting the Fermi energy of CNTs (Figures 3E and 3G). There are three main types of charge-transfer dopants for CNTs. The first type—inorganic molecules—can be divided into donors and acceptors, either according to the relative height of the highest occupied molecular orbital and lowest unoccupied molecular orbital of dopants to the Fermi level of the CNTs or according to relevant reactions of the dopant, such as decomposition and oxidation. The second category involves organic/organometallic molecules or polymers. The doping effect is determined by the relative ionization energies and electron affinities of both the dopants and the CNTs. Third, metals or metal oxides have also been used as dopants, whereby the charge transfer is driven by a mismatch in the work functions of the CNTs and dopants. Kim et al. reported strong charge transfer from SWNTs to $AuCl_3$ via a high level of p-doping.[45] The downshifted work function forces the Fermi level of the SWNTs to be located deep in the valence band.

In general, doping whereby certain atoms or molecules interact (covalently or noncovalently) with the nanotube surfaces is an effective and facile method for tuning

the electronic properties of CNTs, which broadens their range of applications. However, several important issues must be addressed, such as the unavoidable carrier-mobility decrease and how to precisely control the spatial distribution of dopants in CNTs. Additionally, many other energy-band modulation techniques are worthy of attention.

External Electric Field

Previous calculations and experiments have indicated that the electronic and transport properties of CNTs can be modified by a transverse electric field (Figure 3D) if the field strength is large enough to couple the neighboring sub-bands.[46–48] The CNTs may then undergo band-gap opening and closing, energy-band shifting, and sub-band degeneracy lifting. Typically, the unique electronic band structure modification of CNTs under a transverse electric field can be attributed to the sub-band mixing effect.[46] Most armchair CNTs remain metallic under transverse electric conditions, with an increase in the DOS near the Fermi energy (Figure 3I). For quasi-metallic zigzag CNTs, a band gap opens at the Fermi point under weak fields. When the field strength increases beyond a threshold, the gap starts to decrease.[47] A common rule is that CNTs with larger diameters are more sensitive to the external field, because of the smaller energy separation between neighboring sub-bands. Therefore, a larger CNT diameter necessitates a weaker critical field for the initial gap opening and possesses a smaller maximum gap with field strength increasing. Figure 3F shows that for semiconductor zigzag CNTs, the gap decreases monotonically with the increasing transverse electric field strength, ultimately realizing a semiconductor-metal transition. For instance, an external electric field of at least 0.30 V $Å^{-1}$ is required for (10, 0) tubes to undergo a semiconductor-metal transition, an external electric field of 0.20 V $Å^{-1}$ is required for (20, 0) tubes, and an even lower field strength (e.g., <0.05 V $Å^{-1}$) is sufficient for CNTs with larger diameters.[47] This can be attributed to two factors: (1) according to the sub-band mixing theory, the band-edge states move away from the Γ point and eventually cross each other, resulting in a gap closing;[48] and (2) the energy reduction of the hybridized singlet state to the original band gap, which may occur even before the band gap can be affected by the movement of the band edges; such a mechanism is prominent for (n, 0) CNTs with $n < 17$.

The possibility of modulating the band gap in CNTs by using an external electric field, creating additional band-edge states, and destroying the state degeneracy (especially the semiconductor-metal transition in the case of semiconducting zigzag CNTs) widens the range of applications of CNTs in electronic and optoelectronic devices.

Radial Deformation

Similar to the scenario whereby an external field is exerted on CNTs, under a radial deformation, s-CNTs may also transit to metal (Figures 3C and 3F). According to theoretical calculations, the gap of zigzag CNTs closes under uniaxial strain, which is due to σ^*-Π^* hybridization, that is, the downshift of the hybridized singlet state in the conduction bands.[17] In general, electronic states near the Fermi level are essentially Π- or Π^*-derived, but this is not the case for smaller tubes where large σ^*-Π^* hybridization effects occur due to the extremely large curvature. Radial deformation leads to a similar effect,[49] which is universal in (n, 0) CNTs, except for the difference in the relative position of the singlet state with respect to the double-degenerate state. For $n < 9$, the band gaps are closed monotonically with the increasing strain. For $n \geq 9$, the band gaps increase at the initial stages of deformation owing

to a higher rate of downshift of the double-degenerate valence band. Once the singlet Π* band begins to move faster and enters the gap, the gap starts to narrow with the increasing deformation.[47] For armchair CNTs, at a small deformation, the break of mirror symmetry dominates, which can lead to a small band gap of <10 meV (Figure 3H). A gap of ~0.1 eV can be induced when layer-layer interactions become significant at a larger strain. It is worth noting that when mirror symmetry breaking is dominant, breaking all the mirror symmetry planes is necessary to introduce a perceptible gap.

There are additional novel methods, such as the introduction of grain boundaries (GBs).[50] This approach is inspiring because with the introduction of GBs along the tube axis, the CNTs become narrow- or zero-band-gap materials. Thus, there is no need for helicity diameter selection to separate specific CNTs. However, the difficulty of synthesizing these new structures remains a critical limitation for their application.

Construction of Heterostructures

Building junction structures is a common technique in the semiconducting industry. For example, in solar cells and light-emitting devices, the design of p-n junctions significantly reduces the loss of carrier transport and improves the power-conversion efficiency. Heterostructures refer to the special band area formed by the contact of two materials with different band gaps. The band bending and the generation of energy barriers can significantly affect the carrier transport. By designing suitable heterostructures, specific requirements can be satisfied and the device performance can be significantly improved. Semiconductor heterostructures and superlattices have become the material foundation for modern electronics and optoelectronics. Traditional ways for fabricating heterostructures are largely based on the technology of chemical epitaxial growth, physical vapor deposition, or solution processing. The successful isolation of graphene opened the door of the family of two-dimensional (2D) materials and gradually gave rise to a new era of van der Waals (vdW) heterostructures. Typically, vdW heterostructures are physically integrated by low-dimensional materials through weak vdW interactions. Although they originate from 2D layered materials, vdW heterostructures are not limited to interplanar interactions. A mixed-dimensional heterostructure may demonstrate more functions. As 1D nanomaterials with excellent properties, CNTs have been used to build heterostructures with many other functional materials, broadening their applications. In this section, we focus on the synthesis and functions of CNT-based heterostructures.

It is worth mentioning that a single CNT can build a homojunction itself because of the diverse electronic structures of CNTs, which is called an intramolecular junction. In previous studies, CNT intramolecular junctions were demonstrated as two straight segments with kinks, which originated from two different mechanisms: pentagon-heptagon (5-7) topological defect pairs and local mechanical deformation in a uniform nanotube.[51] In further studies, additional methods were developed for introducing intramolecular junctions, mainly including selective doping,[52] mechanical deformation,[53] temperature variation,[54] and post-connecting different SWNTs by welding.[55] However, the structural and chemical stability of CNTs makes it difficult to control the direct formation of junctions and limits their applications. The most widely used intramolecular junctions of CNTs are the p-n and p-i-n junctions formed via the proper doping of transistors and optoelectronics.

Heterostructures are basically designed to modulate the carrier-transport process, including the transport channel, direction, and space (Figure 4A). For CNT-based

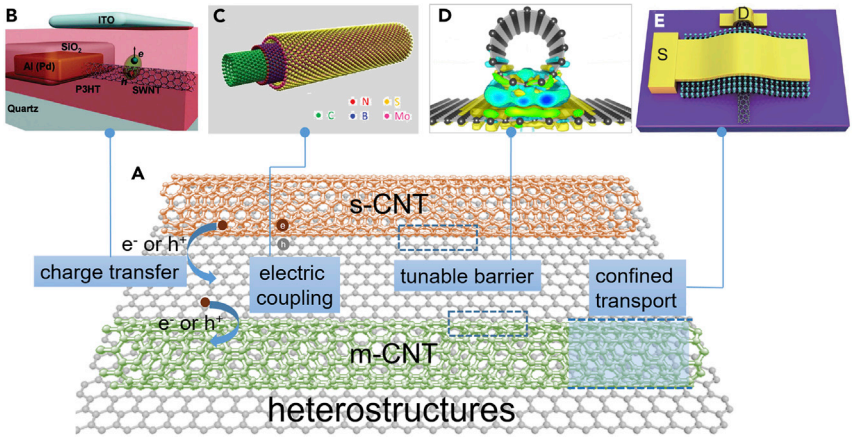

Figure 4. Typical Mechanisms for CNT-Based Heterostructures

(A) Schematic of CNT-graphene heterostructures.

(B) Schematic of the charge transfer in the SWNT-P3HT heterostructured photovoltaic device. Adapted with permission from Dissanayake et al.[56] Copyright 2011, American Chemical Society.

(C) Schematic of an SWNT-BNNT-MoS_2 coaxial 1D heterostructure. Adapted with permission from Xiang et al.[59] Copyright 2020, The American Association for the Advancement of Science.

(D) Schematic of a CNT-graphene interface, showing the charge distribution. Adapted with permission from Cook et al.[60] Copyright 2012, AIP Publishing.

(E) Schematic of a CNT-confined vertical heterostructure. Adapted with permission from Zhang et al.[61] Copyright 2017, John Wiley and Sons.

heterostructures, their functions mostly depend on the charge transfer between the two materials, which improves the effective transport channels in electronics, optoelectronics, and sensors (Figure 4B).[56] Numerous materials have exhibited effective charge transfer with CNTs. Studies on hybrids of CNTs and nanocrystals, including quantum dots (QDs) and nanoparticles, have been performed earlier. The nanocrystals can be decorated on the walls of the CNTs or inside the tubes, which are mainly used in catalysis, optoelectronics, and sensors. The methods for synthesizing CNT-nanocrystal heterostructures can be categorized as *ex situ* and *in situ* techniques.[57] The *ex situ* approach usually requires pre-functionalization of the CNTs; then, the prepared nanocrystals are modified and attached to the surfaces or edges of the CNTs via covalent, noncovalent, or electrostatic interactions. In contrast, in the *in situ* approach, nanocrystals are directly synthesized on pristine or functionalized CNTs via gas-phase deposition techniques, electrochemical techniques, or solution-synthesis methods, among others. Other interesting approaches have been developed in recent years. Palma's group developed a strategy whereby single QDs can be tethered to the ends of individual CNTs in solution with DNA interconnects, forming one-to-one heterostructures. The electronic coupling between CNTs and QDs can be tuned by changing the length of the DNA linkers, which offers new opportunities for synthesizing solution-processable reconfigurable heterostructures for optoelectronics, light harvesting, and sensing applications.[58]

Nanowires and nanotubes of other materials are also integrated with CNTs to form microscopic heterojunctions. According to the positional relationship between the two materials, these junctions can be lengthened, point-contacted, or coaxially stacked. The former two objectives were pursued in early studies and commonly achieved by synthesizing other materials based on the prepared CNTs. For example, Au nanorod/SWNT heterojunctions were obtained via the growth of Au nanorods in solution on a substrate with SWNTs.[62] With the spring up of the vdW heterojunction, coaxially stacked structures have attracted increasing interest. This heterostructure

is usually obtained by using CNTs as a growth template. For example, tubular vdW heterostructures of single-layered PbI_2 within MWNTs were synthesized using laser irradiation and can be used in efficient photodetectors and photoresponsive memory devices.[63] Recently, Xiang et al. reported the fabrication of an SWNT-boron nitride nanotube (BNNT) and SWNT-BNNT-MoS_2 coaxial heterostructures with diameter of <5 nm through low-pressure CVD (Figure 4C).[59] They proposed an open-ended growth mechanism and proved that the BNNT coating did not influence the intrinsic electronic transport of the SWNTs. Further characterization of the SWNT-BNNT-MoS_2 layered structure revealed strong electronic coupling between the SWNTs and the MoS_2, even when they were separated by a few layers of BNNT. This indicates another mechanism of CNT heterostructures: even non-contacted materials, where electrons and holes are spatially separated, can be electronically coupled.

CNTs with 2D material-based heterostructures have been recently investigated because of the increasing use of 2D materials. By fabricating heterostructures based on CNTs and suitable 2D materials, the advantages of both materials can be combined, yielding synergistic effects in device applications. Graphene—a 2D carbon material—is the most popular building block for CNT heterostructures. With regard to the structure, CNT/graphene (CNT/Gr) heterostructures can be either parallel or vertical, according to the geometric relationship between the CNT axis and the graphene plane. With regard to the bonding mode, CNT and graphene can be bonded by either vdW interactions or covalent bonds, referred to as seamless heterostructure.[64] CNT/Gr heterostructures are mostly obtained through the transfer process, growth (CVD), or deposition (e.g., drop-casting) of CNTs on graphene. Because of the diverse electronic structures of CNTs, CNT/Gr heterostructures can exhibit diverse properties according to the structure of the CNTs and the bonding mode. It has been proved both theoretically and experimentally that the heterostructures can provide better mechanical, electrical, and thermal properties than the individual materials. A vertical heterostructure with covalent bonding may result in a band gap in metallic CNTs.[65] The seamless heterostructure is expected to exhibit a significantly higher Young's modulus owing to the sp^3 bonds at the interface.[66] Regarding the energy bands, CNT/Gr heterojunctions can provide tunable barriers at the interface, which depend on the nanotube diameter (Figure 4D).[60] Gangavarapu et al. achieved a barrier-free contact between CNTs and graphene.[67] Another typical 2D material used to build heterojunctions with CNTs is MoS_2. Similar to the fabrication of CNT/Gr heterostructures, the preparation of CNT/MoS_2 mainly involves the transfer process and growth of one material on the other.[68] The role of CNTs in heterostructures depends on the electronic structure of the CNTs used. In particular, SWNTs can be used to construct CNT-confined vertical heterostructures with 2D materials such as MoS_2 (Figure 4E),[61] which have potential for future nanoelectronics.

The aforementioned heterostructures are all based on microscopic interactions with a single CNT. The diverse band structures and high processability of CNTs has led to their widespread use in constructing heterostructures with different materials in different forms, which broadens the range of their application. In addition to microscopic heterostructures using individual nanomaterials, CNT aggregate-based macroscopic heterostructures have also been studied in diverse applications. Among all the CNT aggregates, films are the most widely used due to their easy fabrication process and tunable electrical properties. Suitable doping of CNT films in CNT/Si heterostructures to form p-n junctions is a common approach to improve the exciton dissociation and carrier transport. CNT films have been used as efficient

active and transport materials in optoelectronic devices after the construction of layered heterostructures with other functional materials such as organic semiconductors, C_{60}, perovskite, and graphene. For example, photodetectors based on CNT/Gr film heterostructures exhibit better performance because of their larger active area and broader light absorption range compared with individual materials. Regarding other aggregates, Adams et al. recently reported CNT yarns with organolead triiodide perovskite wrapped as wire-shaped heterostructures, which can be used as self-powering photodetectors with high performance.[69] Wang and Kumta reported the synthesis of heterostructures consisting of CNT vertical arrays and nanoscale amorphous/nanocrystalline Si droplets using a simple two-step liquid-injection CVD process, which has potential for use in high-capacity Li-ion anodes.[70]

Therefore, according to the special band structures of CNTs, proper band engineering based on the target device is necessary. With regard to the different stages before the manufacturing of a device, the enrichment of CNTs with specific electrical properties is essential to satisfy the basic device requirements. Suitable modulation of the energy bands is an alternative method for improving the properties of CNTs for certain functions. In device preparation, the construction of heterostructures is worthy of consideration because they can bring synergetic effects and further improve the device performance. Through rational band engineering, CNTs and their aggregates have played an important role in various electronic and optoelectronic devices.

CNT-BASED MICROSCOPIC DEVICES

In 1965, Gordon Moore predicted that the number of transistors that could be packed into an IC on a chip would double every 18–24 months and that its performance would double as well. This is known as Moore's law. However, with the development of the semiconductor industry, traditional Si-based electronics cannot meet the requirements of smaller and faster devices, and the problems of current leakage, energy loss, and heat are becoming increasingly serious. Moore's law faces failure, and it is urgent to develop new materials for the future. CNTs, together with suitable band engineering, offer hope for a new era in electronics. In this section, we focus on nanoscale-to-microscale CNT devices and integrated systems based on them.

Devices Based on Pure CNTs

FETs

Since the successful acquisition of CNTs and their single-wall structures, numerous theoretical calculations and experimental results predicted their unique electronic structures and excellent transport performance. With the development of material synthesis techniques, device manufacturing has gradually matured, especially for FETs. From single CNT transistors to small-scale logic circuits and then to microprocessors, scientists are moving closer to the goal of developing "beyond-silicon electronic systems" (Figure 5).

Since the first room-temperature FET based on a single CNT was developed in 1998 (Figure 5A),[71] researchers have tried to improve the performance by optimizing the materials and devices. In terms of devices, there are three main routes. The first is the dielectric layer. In 2002, Dai's group integrated high-κ (dielectric constant) dielectric ZrO_2 into SWNT transistors as a gate dielectric layer through atomic layer deposition (ALD)[72] to replace traditional SiO_2 or Al_2O_3[81] (Figure 5B). The high capacitance of ZrO_2 dielectrics results in subthreshold swings of $S \approx 60$–80 mV dec^{-1}, a transconductance of ~6,000 S m^{-1}, and a carrier mobility of 3,000 cm^2 V^{-1} s^{-1} for p-type FETs.[72] The performance was further improved by combining high-κ HfO_2 films as

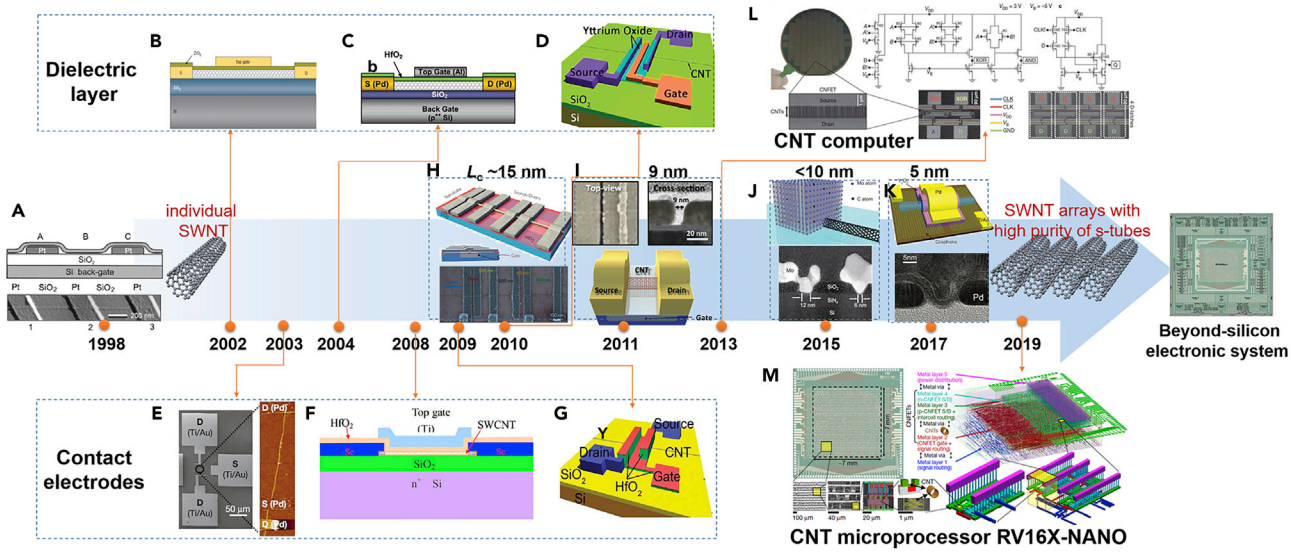

Figure 5. Development History of CNT FETs and ICs

(A) The first CNT FET based on a single semiconducting SWNT. Adapted with permission from Tans et al.[71] Copyright 1998, Springer Nature.

(B–D) FET devices with typical dielectric layer materials.[72–74] Adapted with prmission from Javey et al.[72] Copyright 2002, Springer Nature. Adapted with permission from Javey et al.[73] Copyright 2004, American Chemical Society. Adapted with permission from Wang et al[74]. Copyright 2010, American Chemical Society.

(E–G) FET devices with typical contact electrodes.[6,75,76] Adapted with permission from Javey et al.[75] Copyright 2003, Springer Nature; Adapted with permission from Zhang et al.[6] Copyright 2008, AIP Publishing; Adapted with permission from Javey et al.[76] Copyright 2008, American Chemical Society.

(H–K) Scaling the channel length in CNT FETs.[77–80] Adapted with permission from Franklin et al.[77] Copyright 2010, Springer Nature; Adapted with permission from Franklin et al.[78] Copyright 2012, American Chemical Society; Adapted with permission from Cao et al.[79] Copyright 2015, The American Association for the Advancement of Science; Adapted with permission from Qiu et al.[80] Copyright 2017,The American Association for the Advancement of Science.

(L) CNFET subcomponents in a CNT computer. Adapted with permission from Shulaker et al.[3] Copyright 2013, Springer Nature.

(M) Image of a fabricated RV16X-NANO chip. Adapted with permission from Hills et al.[4] Copyright 2019, Springer Nature.

gate insulators, optimized metal-CNT contacts, and electrostatically doped nanotubes (Figure 5C).[73] Another high-κ dielectric Y_2O_3 was first reported by Wang et al. through direct growth on the surfaces of CNTs without using noncovalent functionalization layers or inducing significant structural distortion and damage (Figure 5D). The CNT FET based on a 5-nm Y_2O_3 top-gate dielectric exhibited an ideal subthreshold swing of 60 mV dec^{-1}.[74]

The second route for performance breakthroughs is contact electrodes. In the early stage of CNT FET research, it was found that when traditional electrodes such as Ni/Au or Ti/Au were used, the devices actually operated as Schottky barrier transistors. The switching behavior depends on the modulation of the contact barrier rather than the channel conductance due to the Schottky contact interface between the semiconducting CNTs and the metals. The current from the junction mainly depends on the thermionic emission and tunneling current under the bias.[82] The transistor operates under gate and source-drain field-induced modulation of the band structure at the contacts.[83] Therefore, the principle to design the contact electrode is to reduce or eliminate the Schottky barriers between the semiconducting CNTs and the metals, and the metals used should have good wetting with CNTs. In 2003, Dai's group greatly reduced the barriers by using the high-work-function metal Pd as a contact with CNTs (Figure 5E), realizing nearly ohmically contacted ballistic transport in semiconducting p-type CNTs.[75] For n-type CNTs, Peng's group performed a series of studies to optimize the contacts. They found that the performance of the n-CNT FET could exceed that of n-type Si FETs when the metal Sc

was used as the contact electrode and HfO_2 was used as the dielectric layer (Figure 5F).[6] By further designing the device with a self-aligned gate structure, the n-CNT FET performance can be improved to nearly ballistic transport.[76] Later, they used the metal Y to replace the expensive metal Sc as the contact electrode (Figure 5G). In this case, an ohmic contact with n-type CNTs was also achieved, and the subthreshold swing of n-FET devices was only ~73 mV dec^{-1}, with an electron mobility of up to 5,100 $cm^2 V^{-1} s^{-1}$.[84]

The last route for device optimization is reducing the scale, which is mostly reflected in the decrease of channel length (L_c). For the aforementioned single CNT FETs, the L_cs were on the order of micrometers to hundreds of nanometers. In 2010, Franklin and Chen reported that CNT FETs maintained their performance with L_c scaling from 3 to 15 nm, without existence of short-channel effects (Figure 5H).[77] They further reduced the L_c to sub-10 nm with Pd contacts and an HfO_2 dielectric layer, yielding an impressively small inverse subthreshold slope of 94 mV dec^{-1} (Figure 5I).[78] In 2015, Cao et al. developed an end-bonded contact scheme whereby the SWNTs were attached to the bulk Mo electrode through carbide bonds, and the contacts exhibited size-independent resistance (Figure 5J). FET based on this contact exhibited a more than 2-fold performance advantage over Pd-contacted device when L_c scaled below 10 nm.[79] In 2017, Peng's group successfully fabricated top-gated CNT FETs with a gate length of only 5 nm (Figure 5K), which outperformed a silicon CMOS device with the same scale. Further optimization of the device with graphene contacts resulted in faster operation with a much smaller subthreshold swing of ~73 mV dec^{-1}.[80] A CMOS inverter with a total pitch size of 240 nm was also fabricated. In 2018, they used graphene as a Dirac source with a control gate, further reducing the power consumption with an average subthreshold swing of 40 mV dec^{-1}.[85]

As indicated by the foregoing achievements, CNTs have the following advantages over other semiconducting materials for the fabrication of FETs. CNTs have high carrier mobility and can carry a high current density.[75] CNTs have structural and chemical stability and are compatible with various oxide dielectric layers.[86] CNTs with nanoscale diameters are easily regulated by the gate voltage, which can inhibit the short-channel effect.[77] CNTs can be doped to be either p- or n-type semiconductors according to the application requirements of the devices. The achievements in single CNT FETs provide a foundation for the development of CNT-based ICs.

ICs

With the development of synthesis techniques—especially the growth of CNT horizontal arrays, preparation of CNT thin films, and separation of semiconductor tubes—great breakthroughs have been made in the fabrication of integrated logic circuits based on CNT FETs. Early in 2001, logic circuits with 2–3 simple CNT FETs were realized by doping of CNTs and circuit design.[72] A circuit composed of two transistors could realize a NOR gate and static random-access memory, and three transistors could be assembled into a ring oscillator. In 2006, a ring oscillator that was composed of 12 transistors and was capable of processing high-frequency signals was developed by using an 18-μm-long SWNT and Pd and Al as the p-gate and n-gate, respectively.[87] In 2013, the first-generation "CNT computer" came out, which consisted of 178 CNT FETs (Figure 5L).[3] CNT horizontal arrays were transferred from the growing substrates directly, and 99.99% of the metal tubes were removed by electrical breakdown. Each transistor was composed of 10–200 CNTs. The CNT computer can perform multiple tasks, such as instruction fetching, data

fetching, arithmetic operations, and write-back. In 2016, a medium-scale IC consisting of 140 p-type FETs was prepared using CNT network thin films prepared from solution. A 4-bit adder and 2-bit multiplier was first realized.[88] In 2017, IBM produced an industrial-scale ring oscillator with a switching frequency of 2.82 GHz using solution-deposited CNT films with semiconductor tubes of 99.9% purity.[89] In 2019, MIT developed a beyond-silicon microprocessor called RV16X-NANO, which was made entirely from CNT FETs and consisted of more than 14,000 CNT CMOS transistors (Figure 5M).[4] The processor used CNT networks deposited from solution-separated semiconducting CNTs of 99.99% purity, and special processes of impurity removal, metal contact interface design, electrostatic doping, and circuit design were used to eliminate the influence of residual metal tubes and improve the device performances. This 16-bit microprocessor can run standard 32-bit instructions on 16-bit data and addresses, operating as modern microprocessors do today. RV16X-NANO is a milestone in the application of CNTs.

It is obvious that the breakthroughs in CNT ICs rely heavily on the progress in material synthesis. As shown in Figure 5, from the first CNT FET to the CNT computer, the material experienced a revolution from single SWNTs to SWNT arrays with high-purity semiconducting tubes. In practical IC applications, each FET channel requires numerous SWNTs to drive the required current, and the extrapolation model from individual CNTs predicts that parallel CNT arrays can perform better than traditional semiconductors.[90] Besides, for high-performance ICs, which may integrate up to billions of FETs in a chip, the content of the metallic tubes must be less than 0.0001%.[39] Recently, a major breakthrough has been made in CNT-array-based electronics.[91–93] The CNT FETs outperformed the commercial silicon-based FETs with similar gate length based on preparation of aligned semiconducting CNT arrays with high density (100–200 CNTs/μm) through a multiple dispersion and sorting process and a dimension-limited self-alignment procedure.[91] DNA-templated approaches were also used as promising strategies to obtain semiconducting CNT arrays and devices with high performance.[92,93] Therefore, developments in the preparation of high-density CNT horizontal arrays or films, and techniques for the selective enrichment of semiconducting tubes, gave rise to recent achievements in CNT ICs and pave way for the next generation of beyond-silicon electronics.

Radiofrequency and Memory Devices

CNT-based FETs are the most basic devices for applications in the electronic field. Further design and optimization can expand their functions, e.g., radiofrequency (RF) and memory, which are also important components for highly integrated, multifunctional chips.

RF technology is the basis of high-speed wireless communication. With the development of modern electronic equipment, the integration of separate technology has become increasingly important, including the requirement for advanced functions such as processing complex RF front ends. In the current semiconductor industries, although excellent performances have been achieved in GaAs pseudomorphic high-electron-mobility transistors, the preparation process of the bulk materials is complex and incompatible with Si CMOS integration technology. As mentioned previously, CNTs have high carrier mobility with quasi-ballistic transport performance, and their preparation process is highly compatible with other device technologies. Their 1D structures have been verified to have highly linear signal amplification performance.[94] In 2007, Zettl's group reported the first CNT radio, which comprised a single CNT and featured all the essential components of a radio operating in the 40–400 MHz range, including antenna, tunable band-pass filter, amplifier, and demodulator. However,

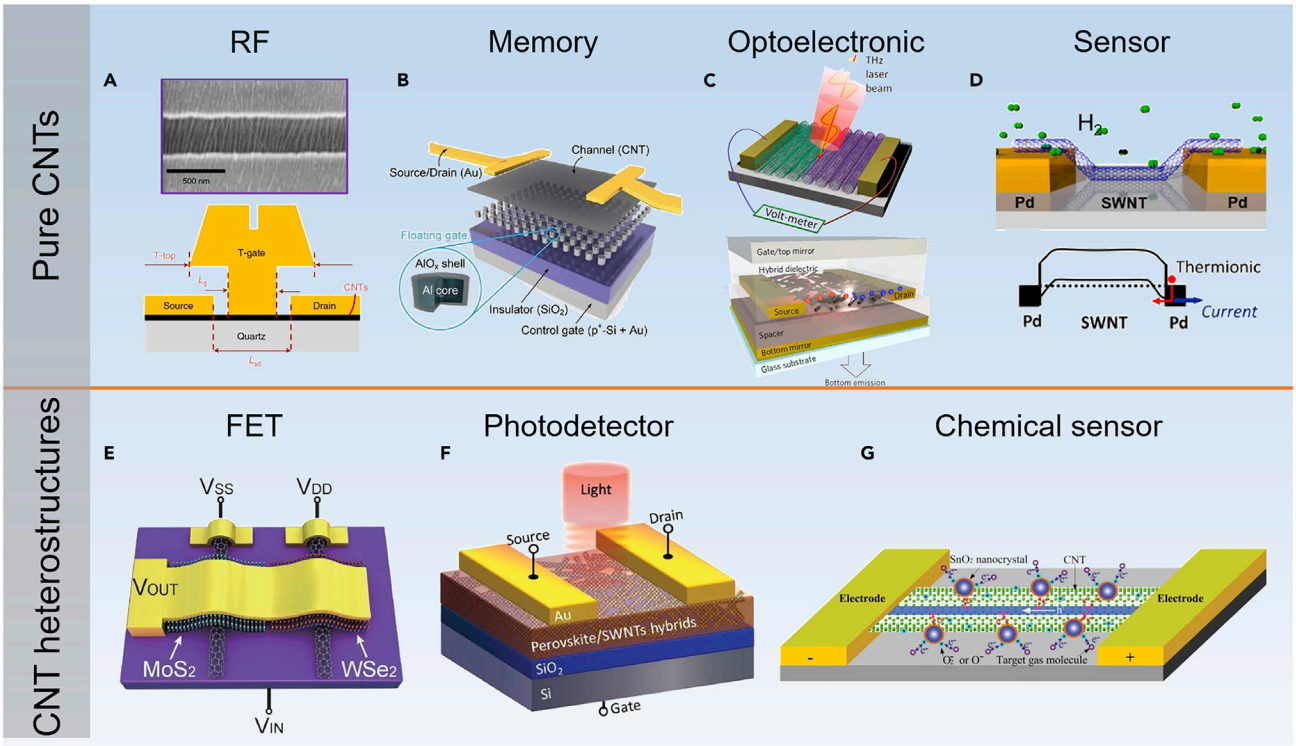

Figure 6. Other CNT-Based Microelectronic Devices

(A) CNT array-based RF devices with a T gate. Adapted with permission from Rutherglen et al. [97] Copyright 2019, Springer Nature.

(B) Schematic of a CNT nonvolatile memory transistor with Al nanoparticle-based floating gate. Adapted with permission from Qu et al.[98] Copyright 2020, John Wiley and Sons.

(C) Schematic of a CNT-based THz detector (top)[99] and a bottom-contact/top-gate light-emitting FET (bottom).[100] Adapted with permission from He et al.[99] Copyright 2014, American Chemical Society; Adapted with permission from Graf et al.[100] Copyright 2017, Springer Nature.

(D) Schematic of the device and mechanism of a CNT H_2 sensor. Adapted with permission from Salehi-Khojin et al.[101] Copyright 2011, American Chemical Society.

(E) Schematic of a CNT-confined vertical heterostructure-based FET. Adapted with permission from Zhang et al.[61] Copyright 2017, John Wiley and Sons.

(F) Schematic of a phototransistor based on CNT-perovskite heterostructures. Adapted with permission from Wu et al.[102] Copyright 2017, John Wiley and Sons.

(G) Schematic of a gas sensor based on CNT-SnO_2 heterostructures. Adapted with permission from Lu et al.[103] Copyright 2009, John Wiley and Sons.

the equipment functioned at least in part mechanically, which relied on the physical vibrations of the charged tip after electromagnetic-wave transmission impinged upon the tube.[95] The performance of CNT RF transistors has been continuously improved with the improvement of the fabrication technology of CNT arrays and the skills to enrich the semiconducting tubes. Zhou's group prepared an RF transistor by using CNT horizontal arrays grown through CVD and the design of a T-shaped gate.[96] The CNT arrays ensured good transport, and the T-gate reduced the parasitic capacitance and resistance of the gate, both contributing to the improved performance of an extrinsic current-gain cutoff frequency of 25 GHz and an intrinsic current-gain cutoff frequency of up to 102 GHz. In 2019, Rutherglen et al. used solution-separated CNTs with a semiconducting content of 99.9% and a floating evaporative self-assembly process to prepare a dense CNT horizontal array at the wafer scale. With a T-gate design having a 110-nm gate length (Figure 6A), the device exhibited an extrinsic cutoff frequency of over 100 GHz, which surpasses the 90 GHz of the RF CMOS device.[97]

Memory devices are generally classified into nonvolatile and volatile memory. The two types of memory can be realized by controlling the charge recombination rate

through device design. In general, storage functions are implemented by designing a gate oxide[104] or a passivation layer[105] of CNTs to trap charges. Recently, Qu et al. developed a flexible CNT nonvolatile memory transistor called sen-memory.[98] The active channel was formed by a CNT thin film with a semiconducting content of 99.9% separated by the solution method. The excellent memory performance of the device was mainly realized by the Al nanoparticle-based floating gate (Figure 6B). Holes can be easily trapped by Al, whose discrete-nanoparticle structures can impede the lateral charge accumulation. Additionally, the ultrathin AlO_x coating can reduce the loss of trapped charge. At the same time, the AlO_x tunneling layer can remove the charges trapped in the floating gate and return to the channel by direct tunneling when the irradiation energy is higher than the work function of Al, resulting in a significant improvement in the off-state. The sen-memory device realized a new multifunctional system integrating image sensing and information memory.

Mentioned above are typical microelectronic devices based on pure CNTs. In addition, the direct-band-gap structure of semiconducting CNTs and the tunable band structures of CNTs make them potential candidates for use in optoelectronic devices.

Photodetectors and Light-Emitting Devices

Photodetectors convert optical signals into electrical signals and are widely used in environmental monitoring, the military, imaging, and so on. To improve the photodetection performance, the active materials should possess strong light absorption and high carrier mobilities. CNTs have a large absorption coefficient (up to 10^4–10^5 cm^{-1} from near-to mid-infrared) and broad absorption spectral range (from UV to terahertz [THz]) because of both the intraband and interband transition processes.[106] Therefore, CNTs are among the most promising materials for photodetectors. The mechanism of photocurrent generation in semiconducting CNTs differs from that in metallic tubes. In metallic tubes, photoexcited hot carriers contribute the current while in semiconducting tubes, photogenerated electron-hole pairs separated under a built-in electric field and then contribute the current.[107] However, photogenerated electron-hole pairs in CNTs have large binding energies (up to several hundred meV, and inversely dependent on the diameter) and exist as excitons instead of free carriers, which is one of the biggest challenges in CNT photodetectors. Thanks to the efforts of researchers, breakthroughs have been made in photodetectors based on CNTs.

Pure CNT photodetectors can be classified into thermal or photo effects according to their photo-to-current mechanism. Thermal effect-based photodetectors include thermopile and bolometers, in which the temperature change caused by light irradiation results in a current change. The current signals come from the resistance change caused by lattice phonons, which obtain the energy from irradiation but not from photoexcited band transitions. The performance of the device is easily affected by the surrounding environment, so only CNTs suspended in vacuum can show obvious responses.[108] Generally speaking, the dark current of thermal effect detectors is large and the signal-to-noise ratio is poor. Photo-effect-based detectors typically include photoconductive devices, and photodiodes or transistors composed of p-n junctions and heterojunctions, in which the response signals are caused by the transition of electrons and the output signal can be photocurrent or photovoltage. Although a single CNT can also produce an obvious photovoltage with asymmetric electrodes,[109] the effective area is small and the light absorption is limited. Therefore, CNT arrays or films are more suitable for photodetectors. CNTs have relatively small dark currents compared with materials such as graphene,

so they can realize infrared detection at room temperature. Peng's group fabricated a high-performance room-temperature infrared detection transistor by using a CNT horizontal array film assembled from solution-separated high-purity semiconducting tubes and asymmetric Sc-Pd electrodes, which preliminarily realized infrared imaging through integration. The device exhibited fast response, excellent stability and uniformity, ideal linearity, and low energy consumption.[110] Typical voltage response detectors can also be fabricated using CNT diodes with asymmetric electrodes. Further construction of a cascading device comprising virtual contacts connecting several diodes in series can double the voltage signal.[111] In addition, due to the special 1D structure and anisotropy of CNTs, they can also be used to detect polarized light. Fan's group fabricated a photodetector based on a freestanding superaligned CNT film spun from those grown by low-pressure CVD. The device showed different responses to different light wavelengths regardless of the light intensity because of the different absorption behavior with respect to the polarization angles.[112] He et al. prepared a THz detector by using CNT horizontal arrays and n-type doping to obtain p-n junctions (Figure 6C top). The device requires no additional bias, can realize broadband detection at room temperature, and is sensitive to polarized light.[99] In recent years, to integrate into the modern society, CNT photodetectors have gradually developed in the direction of flexible and wearable devices, such as fully printed flexible CNT photodetectors[113] and CNT textile photodetector fibers, which can be woven into clothes.[114]

As semiconductors with high mobilities, CNTs can also be used to prepare light-emitting devices, and the infrared emission is dominated according to their band gaps. Considering the light-emission mechanism, CNT-based emitters can depend on undoped electron-hole injection, doped p-n diode electroluminescence, and defect luminescence. Avouris' group prepared a long-channel light-emitting FET using a single undoped CNT.[115] Recombination occurs when two types of carriers meet and form a short ambipolar segment because the abrupt metal-nanotube contacts allow the injection of electrons and holes and then emit infrared light. The emitting location can be controlled by varying the gate and drain voltages. They further developed a CNT light-emitting diode by using an electrostatic doping technique. Two gates were designed to control a single CNT, which reduced the energy consumption by a factor of up to 1,000 and resulted in high carrier-to-photon conversion efficiencies and a narrow emission spectral range (~35 meV).[116] He et al. realized single-photon emission at sp^3 defect sites with modulated spectral by chemical modification of SWNTs. Aromatic functional groups were introduced onto the wall of SWNTs through diazotization for exciton localization at the defect sites, and single-photon emission with a purity of up to 99% at room temperature was achieved. In addition, by doping CNTs with different chiral indices, which were separated from the solution, the emission wavelength could be adjusted between 1.3 and 1.55 μm.[117] Along with solution-processed semiconducting (6, 5) SWNTs, Zaumseil's group prepared microcavity-integrated light-emitting FETs (Figure 6C, bottom) and realized efficient electrical pumping of exciton-polaritons at room temperature with high current densities and tunable wavelengths in the range of 1,060–1,530 nm.[100]

Chemical Sensors

Owing to the excellent electrical properties and large surface area-to-volume ratio of CNTs, CNT-based devices show great sensitivity to many analytes and thus are widely used in chemical sensors. CNT-based chemical sensors include gas sensors and biological sensors, which are important for environmental monitoring, food safety, and medicine. There are three main sensing mechanisms for CNT-based chemical sensors according to the interaction sites of the analyte: the intra-CNT

effect, the inter-CNT effect, and the junction effect (occurring at the junction between the CNTs and the electrodes). The intra-CNT effect refers to the charge transfer between the analyte and the CNTs, which leads to the change of carrier concentration in CNTs or the generation of defects on CNT walls.[118] For example, for commonly p-doped CNT FETs under ambient conditions, the adsorption of electron-donor molecules such as NH_3 leads to a loss of holes, yielding a negative shift in the transfer curve. In contrast, if they are exposed to an atmosphere of electron acceptors such as NO_2, the transfer curve shows a positive shift.[119] For devices consisting of CNT networks, small changes acting at the overlaps between CNTs can change the contact resistance and significantly influence the overall electronic properties (the inter-CNT effect), e.g., filling the gap between the tubes or changing the morphology of the polymers wrapped outside the CNTs. Ishihara et al. found that if SWNTs were wrapped with some metal-polymer, the contact with an electrophilic analyte could cause depolymerization, causing originally isolated SWNTs to make contact and increasing the overall conductance by 5-fold.[120] The junction effect refers to the change in the Schottky barriers when the analyte acts on the device (Figure 6D).[101] The junction effect is sometimes difficult to distinguish from the intertube effect. After performing a series of experiments and simulations, Schroeder et al. pointed out that for CNT networks with high purity, no defects, and high conductance, the sensing behavior is dominated by the electrode-tube junction effect, while for defect-rich CNTs with low conductance the device response is dominated by intra-tube effects.[121] Based on the aforementioned sensing mechanism, single CNTs, functionalized CNTs, and CNT networks are all active in chemical sensors. The device architectures for CNT-based sensors are mainly transistors, two-electrode conductive devices, electrochemical sensors, and device arrays. Up to now, CNTs have been used for sensing gases such as NO_2, H_2, CO, NH_3, H_2S, SO_2, benzene, toluene, and O_2. They have also been used in biosensors, e.g., for the detection of volatile organic compounds such as acetone[122] and of DNA and glucose.[123]

Devices Based on CNT Heterostructures

Band engineering of heterostructures is effective for overcoming some of the limits of pure CNTs and improving the device performance. With the development of new functional materials, FETs based on CNT heterostructures have shown potential for applications. CNTs with different electrical properties can play different roles. Semiconducting CNTs were used to fabricate p-n heterojunction diodes with single-layer MoS_2.[124] The electrical characteristics of this vertical-stacked heterojunction can be tuned by changing the gate bias to achieve a wide range of charge-transport behaviors ranging from insulating to rectifying and can give an efficient and fast response to optical irradiation. A CNT-confined vertical heterostructure was developed by sandwiching 2D MoS_2 or WSe_2 between an individual metallic SWNT and a metal electrode (Figure 6E).[61] The asymmetric contacts gave the heterostructure more distinctive transport properties, such as asymmetric output characteristics and tunable junctions, which show promise for applications in future nanoelectronics.

For optoelectronic applications, the construction of heterostructures aims to improve the device performances, which is mostly reflected in photodetectors. Typical heterostructures used in CNT-based photodetectors are CNT/Gr, CNT/C_{60}, CNT/Si, and CNT/perovskite. Liu et al. transferred CVD-grown graphene onto an ultrathin layer of SWNTs, and the 1D-2D hybrid film shows broadband light absorption in the wavelength range of 400–1,550 nm.[125] The phototransistor fabricated using this film exhibited a high photoresponsivity of 4,100 A W^{-1}, a large photoconductive gain of $\sim 10^5$, and a fast response to illumination, because of the effective separation of electron-hole pairs at the interfaces, effective charge transfer,

and reduced recombination of spatially isolated carriers. CNT/Gr heterostructures can be further used in flexible photodetectors.[126] Park et al. prepared a phototransistor using the SWNTs/C_{60} heterojunction as the active layer. C_{60} can help the photoexcitons in the CNTs to dissociate and accept electrons from the CNTs. The trap of the transferred electrons results in a large photocurrent gain.[127] Li et al. reported a phototransistor based on perovskite films coupled with embedded SWNTs (Figure 6F).[102] They directly mixed the solution-purified (7, 6) tubes into a perovskite precursor solution, which is an excellent stabilizer for the homogeneous dispersion of the CNTs. The introduction of CNTs significantly improved the hole mobility of the spin-coated perovskite film, and the phototransistor exhibited an ultrahigh detectivity of 3.7×10^{14} Jones and a responsivity of 1×10^4 A W^{-1}.

Although many researchers have reported the use of pristine CNTs in chemical sensors, the incorporation of metal nanoparticles is found to sometimes produce specific or stronger responses. Kong et al. modified the CVD-grown SWNTs with ~0.5-nm Pd nanoparticles via electron-beam evaporation. The Pd/SWNTs heterostructures exhibited a significant electrical conductance modulation upon exposure to H_2 in air at a 4- to 400-ppm level at room temperature. The high sensitivity originated from the change in the work function of Pd when H_2 dissociated on Pd and caused electron transfer from Pd to CNTs.[128] Lu et al. fabricated a gas sensor using heterostructures consisting of MWNTs and SnO_2 nanocrystals (Figure 6G).[103] This hybrid sensor exhibited room-temperature sensing capability to low-concentration NO_2, H_2, and CO gases. Compared with the high-temperature sensing of SnO_2 alone and the insensitivity to H_2 and CO for pure CNTs, the good performance of the heterostructure sensor can be attributed to the effective electron transfer between the SnO_2 and the CNTs and the increased surface area of the hybrid nanostructures.

CNT-BASED AGGREGATES FOR MACROSCOPIC DEVICES

Considerable efforts have been made to fabricate various macroscale CNT assemblies with different dimensions, such as 1D fibers, 2D films, three-dimensional (3D) powders, aerogels, and sponges. Aside from the maintenance of uniqueness of individual CNTs, CNT assemblies—whether pure or combined with other materials—have remarkable properties, making them attractive for numerous intriguing applications.

Devices Based on Pure CNTs

Applications of CNT Films

Figure 7 presents the typical preparation methods and applications of CNT films. CNT thin films, including horizontal arrays and networks (Figure 7A), have multiple functions and excellent electronic and mechanical properties. With the constant advancements in electronics, devices are required to be flexible, transparent, and stretchable, and CNT thin films with great processability, stretchability, and stability are promising. Nevertheless, the fabrication technology for flexible devices is still far from rivaling that for rigid devices, owing to the limitations of the processing and manufacturing on flexible substrates. In this section, we review representative applications where CNTs are used as channels for thin-film transistors (TFTs) (Figure 7B) and as transparent conducting films (TCFs) (Figure 7C).

TFTs are fundamental components for panel display in variable modern electronics and can be used to fabricate large-area logic circuits and optoelectronic devices. Similar to the development of FETs, CNT-based TFT development has seen the following trends: the optimization of dielectric and electrode materials, reduction

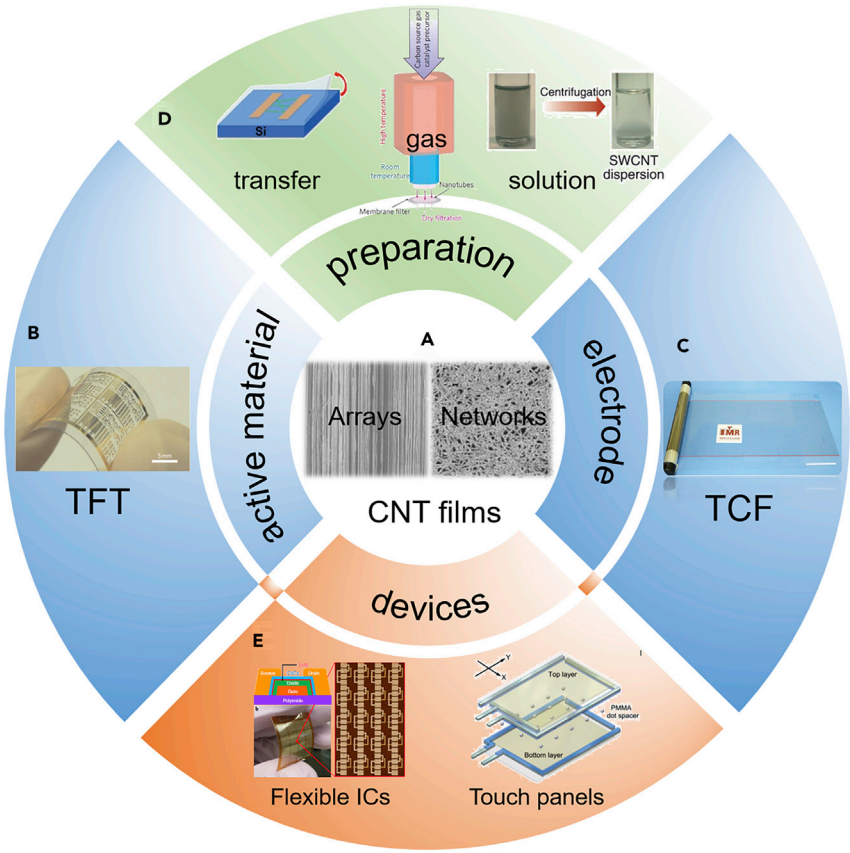

Figure 7. Preparation and Applications of the CNT Films

(A) SEM images of CNT horizontal arrays and networks.

(B and C) Images of CNT-based (B) TFT[129] and (C) TCF.[130] Adapted with permission from Sun et al.[129] Copyright 2011, Springer Nature; Adapted with permission from Wang et al.[130] Copyright 2018, John Wiley and Sons.

(D) Typical preparation methods for CNT films.[129,131,132]Adapted with permission from Thanh et al.[131] Copyright 2012, John Wiley and Sons; Adapted with permission from Okimoto et al.[132] Copyright 2010, John Wiley and Sons; Adapted with permission from Sun et al.[129] Copyright 2011, Springer Nature.

(E) Devices based on CNT films.[133,134] Adapted with permission from Tang et al.[133] Copyright 2018, Springer Nature; Adapted with permission from Feng et al.[134] Copyright 2010, John Wiley and Sons.

of the sizes, large-scale integration, and improved quality of CNT films. According to the CNT film preparation methods, the TFT manufacturing techniques can be classified into three types: solid-phase fabrication, liquid-phase fabrication, and gas-phase fabrication (Figure 7D). Solid-phase fabrication involves microprocessing CNTs directly synthesized from CVD and transferring the products to a target substrate as a whole.[131] For instance, Cao et al. fabricated random networks of SWNTs along with source-drain electrodes and then transferred them to a polyimide substrate.[135] After subsequent processing, ICs comprising up to 100 transistors were obtained on plastic substrates. The transistors exhibited carrier mobilities as high as 80 $cm^2\ V^{-1}\ s^{-1}$, subthreshold slopes as low as 140 mV dec^{-1}, on/off ratios as high as 10^5, operating voltages less than 5 V, and good mechanical flexibility. Thus, the transfer technique is important for optimizing the properties of such devices. Additionally, CNT films can also be deposited from liquid-phase fabrication, including drop-coating, evaporation self-assembly, and printing. Takenobu's group

manufactured SWNT strips with a tunable thickness and tunable coverage, as well as printable ionic-liquid gate dielectrics, via precisely controlled inkjet printing.[132] The fabricated transistors had on/off ratios as high as 10^4–10^5. Moreover, through surface modification of the substrates, such as introducing a (3-aminopropyl)triethoxysilane self-assembly layer, CNT films can be prepared by immersing the substrates in a specific CNT dispersion and used to fabricate TFTs.[136]

To minimize the contamination or degradation of CNTs, directly depositing CNTs synthesized by the floating-catalyst CVD (FCCVD) method onto the substrates is desirable. This gas-phase fabrication technique is facile and continuous but requires further control over the structures of the CNTs. Using FCCVD synthesis and transfer process, Sun et al. manufactured CNT-based TFTs (Figure 7B) with carrier mobility as high as 35 $cm^2 V^{-1} s^{-1}$ and on/off ratios of 6×10^6. They further integrated them into a flexible 21-stage ring oscillator.[129] Zhang et al. fabricated TFTs consisting of pure CNTs by using SiO_x (with a tunable oxygen content) as catalysts.[137]

In CNT-based TFTs, the interaction between individual CNTs, the purity of the semiconducting CNTs, and their diameter, length, and so forth all have great influence on their performance. In 2018, Tang et al. fabricated a CNT-based CMOS on a polyimide substrate via drop-coating of CNTs with semiconducting purity as high as 99.99% (Figure 7E, left).[133] The TFT gave an excellent performance with high current densities (>17 $\mu A\ \mu m^{-1}$), large current on/off ratios (>10^6), and small subthreshold slopes (<200 mV dec^{-1}). The aforementioned TFTs mainly comprised CNT networks; however, theoretically, high-density horizontal CNT arrays are much better for high-performance electrical devices. Unfortunately, they have not been widely used because of limited density and productivity of CNT arrays. Pre-processing before device fabrication to realize CNT arrays with horizontally high density or superalignment may be a solution. For instance, Peng's group utilized a directional shrinking transfer method to significantly amplify the density of the CNT arrays. Using the same technique, they successfully aligned the random oriented CNT films deposited from solution, and the resulting TFTs exhibited enhanced performance.[138]

In addition to TFTs, CNT films and their composites have been widely investigated in the field of flexible electronics as transparent conducting electrodes. Over the past decade there has been an increase in devices that require one or more TCFs, such as touch panels[134] (Figure 7E, right). The material most widely used today for transparent electrodes is indium tin oxide (ITO). However, ITO has problems, for example, its high price due to scarcity and its natural brittleness; thus, it fails to satisfy the requirements of low-cost and flexible electronics in the future market. For next-generation flexible TCFs, CNTs are perhaps the most promising materials due to their unique electronic and optical properties as well as their high stability and excellent mechanical flexibility. The two main figures of merit of TCFs are their sheet resistance and transmittance, which require the networking CNTs to be long and uniform, to have large diameters, and to have high content of metallic tubes and few junctions. Similar to TFTs, there are wet and dry methods for fabricating CNT-based TCFs. The wet method refers to depositing films from a CNT dispersion. Multiple approaches have been utilized, including vacuum filtration, drop-casting, spin-coating, spray-coating, and dip-coating. However, the use of surfactants and subsequent sonication post-processing are usually inevitable to retain the conductivity of TCFs, which brings damage and impurities to the CNT films. To alleviate this problem, Pasquali's group dissolved pristine CNTs in chlorosulfonic acid (CSA) to fabricate transparent conductive CNT films via dip-coating, followed by CSA removal

through coagulation and washing, without surfactants, functionalization, or sonication. The resulting uniform films with high-quality and long CNTs exhibited excellent optoelectrical performance, with a sheet resistance as low as ~100 Ω sq^{-1} at ~90% transmittance in the visible range.[139] The dry method mainly refers to FCCVD to obtain CNT aerogels, but the merits of the facile post-process can be compromised by the difficulty of precisely controlling the synthesis conditions and the difficulty of mass production. Recent years have witnessed great progress in the dry method, including studies on the length, diameter, bundles, and interconnections of CNTs. For instance, Jiang et al. reported that the SWNTs prepared through FCCVD were welded by graphitic carbon and exhibited reduced Schottky contacts between the metallic and semiconducting tubes.[140] The contacts were even converted into near-ohmic ones because of the reduced contact resistance and amount of bundles. The CNT films possess a record-low sheet resistance of 41 Ω sq^{-1}, and 90% transmittance for 550-nm light, which was further reduced to 25 Ω sq^{-1} after HNO_3 treatment. Furthermore, a continuous process including FCCVD synthesis, deposition, and transfer was reported for the fabrication of meter-scale SWNT thin films on flexible substrates. The films showed an excellent performance of a sheet resistance of 65 Ω sq^{-1} and a transmittance of 90% at 550 nm.[130]

Notably, in both the wet and dry methods, doping is important for enhancing the conductivity of the TCFs by increasing the carrier concentration and ameliorating the intertube barriers in CNTs. Dopants typically include NO_2, H_2SO_4, HNO_3, $SOCl_2$, and $AuCl_3$ and immersion in a doping solution is a common approach. Doping does not affect the transmittance of TCFs, and the doping effect is closely related to the chirality distribution of the pristine CNTs.[141] In addition, compositing with other conducting materials, such as metals (nanoparticles or nanowires), conducting polymers, and graphene, has proved to be beneficial for better performance. Wang's group grafted functionalized modified Ag nanoparticles on the surface of the double-walled CNTs (DWNTs) to fabricate TCFs, which exhibited a sheet resistance of 53.4 Ω sq^{-1} with 90.5% optical transmittance at wavelength of 550 nm. The increased performance resulted from the increase in the contact area between DWNTs and the increase in the work function due to the grafting of the Ag nanoparticles.[142] Coleman's group mixed CNTs with a conducting polymer (PEDOT:PSS) and obtained TCFs with a sheet resistance of ~75 Ω sq^{-1}.[143] The TCFs can serve as electrodes for TFTs and thin-film solar cells, as well as essential components of touch screens, displays, and luminescent devices.

Applications of Other Aggregates

Because of the quasi-1D nature of CNTs, one of the most attractive ideas for application of CNTs is that of next-generation electrical transmission lines (Figure 8A).[144–147] Ideally, electrons move ballistically down nanotubes, and the conductivity of these nanotube cables is marginally affected by the temperature. One way to reduce the resistance of transmission lines, which is derived from the scattering of electrons in GBs or junctions, is partial doping. Through post-processing, Zhao et al. fabricated I-doped DWNT cables with an electrical resistivity reaching ~10^{-7} Ω·m, and the specific conductivity (conductivity/weight) of these cables is higher than those of copper and aluminum.[147] The chemically bonded I acted as an acceptor, forming $(I_3)^-$ and $(I_5)^-$ polyiodide chains in the intercalated sites, while mobile holes were created in the DWNTs. Therefore, improved electrical conductivity was imparted to the cables. In addition, considerable research has been directed toward the direct fabrication of CNT fibers, especially from pure metallic CNTs, such as spinning fibers from FCCVD, with a critical control of sulfur promoter,[148] optimization of the flow rates of the carbon source and hydrogen, and appropriate reactor design.[149] The unique electrical

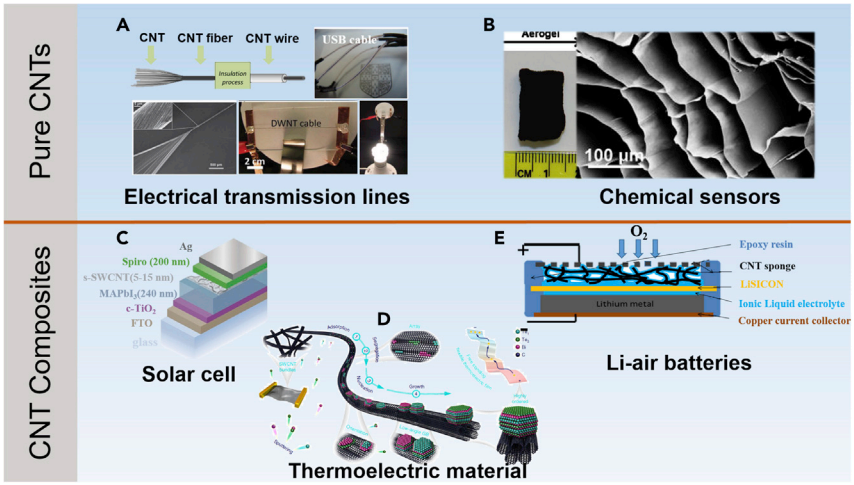

Figure 8. Other Electrical Applications Based on CNT Aggregates

(A) Images of electrical transmission lines made of CNT wires.[144–147] Adapted with permission from Kurzepa et al.[144] Copyright 2013, John Wiley and Sons; Adapted with permission from Ma et al.[145] Copyright 2009, John Wiley and Sons; Adapted with permission from Janas et al.[146] Copyright 2014, Elsevier; Adapted with permission from Zhao et al.[147] Copyright 2011, Springer Nature.

(B) Images of MWNT aerogels for chemical sensors. Adapted with permission from Zou et al.[153] Copyright 2010, American Chemical Society.

(C) Schematic of a perovskite solar cell with CNT films as the hole-transport layer. Adapted with permission from Ihly et al.[154] Copyright 2016, The Royal Society of Chemistry.

(D) Fabrication of layered chalcogenide-SWNT flexible materials for thermoelectric performance. Adapted with permission from Jin et al.[155] Copyright 2018, Springer Nature.

(E) Pd-loaded CNT sponge used in Li-air batteries. Adapted with permission from Shen et al. [156] Copyright 2013, Elsevier.

properties of CNTs, along with resistance to high temperatures and harsh chemical conditions, are useful for practical applications, such as USB[146] and Ethernet cables.[144] On the other hand, CNT fibers are also promising for many applications in electrochemical devices, such as microelectrodes,[150] supercapacitors,[151] and actuators.[152]

Regarding CNT 3D aggregates, pure CNTs can form sponges or aerogels and are used as electrodes or chemical sensors (Figure 8B),[153] but most of them are combined with other materials to maximize the utilization of their unique properties in various fields, as discussed in the next section.

Devices Based on CNT Heterostructures and Composites

Solar Cells Based on CNT Film Heterostructures

Solar energy is an inexhaustible source of clean energy, and solar cells, which can convert solar energy into electricity, are important for alleviating the energy and environmental crisis faced by modern society. CNTs are among the promising materials in solar cells because of their excellent optical and electrical properties. In solar cells, CNTs are mainly assembled in the form of thin films or blended in the active layers, functioning as a charge-transport layer or as an electrode interfacial layer to extract charge (Figure 8C).[154] CNT films with different band structures can be obtained through doping, which can build heterostructures with other active materials and result in effective charge separations. Here, we focus on the role of CNT films in the active layer and the transport layer, that is, photovoltaic devices based on CNT heterostructures. CNTs can be applied to different types of solar cells, including Si solar cells, dye-sensitized solar cells,[157] organic solar cells,[158] and perovskite solar

cells,[154] depending on the active-layer material. Among these solar cells, Si-CNT solar cells are the most systematically studied. The device structure of Si-CNT solar cells is based on oxide-coated Si with a lithographically defined window in the oxide framed by a front-side metal electrode and a rear metal electrode. A CNT thin film is covered over the active area, making contact with the Si in the window as well as the front-side metal, and the device is often mounted on a solid metal support made of steel or copper.[7] The absorption of solar energy mainly occurs in the Si layer, and the photoinduced excitons diffuse to the Si/CNT interface and dissociate under a built-in electric field. Regarding the work mechanism of Si/CNT solar cells, in addition to the p-n junction, researchers also proposed that the fundamental mechanism is either the Schottky junction (CNTs as metal) or the conductor-insulator-semiconductor (CNTs as conductor) junction.[7] For CNT films, the device performance can be improved by using longer tubes and reducing the overlap of CNTs, as well as through appropriate doping. Cheng's group slightly fluorinated CNT films obtained by FCCVD to form a controllable p-type doping, which improved the electrical conductivity and increased the work function of the CNT film and optimized its interface with Si. The solar cells achieved a power-conversion efficiency of 13.6%.[159] Tune et al. prepared Si-CNT solar cells through a new doping protocol based on the outstanding electron-withdrawing properties and excellent Si surface-passivation ability of Nafion. The optimized solar cells achieved breakthrough performance of power-conversion efficiencies of 17.2% and 15.5% for devices with effective areas of 1 and 5 cm^2, respectively.[160]

Thermoelectric and Other Devices

CNT-based thermoelectric composites include CNTs coupled with insulating or intrinsically conductive polymers and CNT-inorganic thermoelectric materials. CNT-polymer composites combine the low thermal conductivity of polymers and the high electrical conductivity and high Seebeck coefficient of CNTs, resulting in high thermal stability. However, the thermoelectric performances of these CNT-polymer composites are still much lower than those of traditional inorganic materials, mainly due to the poor dispersion of CNTs in the polymer matrix. Template-directed *in situ* polymerization combined with layer-by-layer (LBL) deposition can produce well-dispersed polymer/organic nanocomposites with highly ordered structures. Cho et al. synthesized multilayer nanocomposite thin films with graphene and DWNTs stabilized by PEDOT:PSS using LBL deposition.[161] A 1-μm-thick film exhibited a power factor of 2,710 $\mu W \cdot m^{-1} \cdot k^{-2}$, which is the highest ever reported (for any material) at room temperature. The high performance was attributed to the strong interfacial π-π interactions and the 3D interconnected structure. Excellent mechanical flexibility and high thermoelectric performance are also imparted to the composites comprising inorganic nanocrystals and CNTs. Jin et al. recently fabricated layered chalcogenide-SWNT flexible materials with ultrahigh thermoelectric performance (Figure 8D).[155] The Bi_2Te_3-SWNT composites exhibit a power factor of approximately 1,600 $\mu W \cdot m^{-1} \cdot k^{-2}$ at room temperature, which is comparable with that of bulk Bi_2Te_3. Bi-Te adatoms were deposited and preferentially agglomerate at the grooves between the SWNT bundles. The high themoelectric performance of the Bi_2Te_3-SWNT composites arises from the unique, highly ordered structure. The high density of low-angle GBs accounts for the high electrical conductivity and suppresses the scattering of the carriers. Because the thermal conductivity of the SWNTs is dominated by phonons, Bi_2Te_3-SWNT hybrids containing a high density of multiscale defects, such as Te vacancies, GBs, and stacking faults, can scatter phonons, helping to limit the thermal conductivity.

Thanks to the extraordinary properties inherited from their components, CNT-based composites are promising for various other applications, such as electrodes,

conductive additives, and catalysis. Zhang's group reported a series of flexible fibers based on CNTs, silk composites, which can be further weaved into sensors and supercapacitors.[162–164] CNT-based aerogels, which are usually obtained in sol-gel processes, mixed with specific polymers/binders,[165] or grafted with functional groups, can serve as conductive additives in electrode materials for supercapacitors,[166] providing a large specific surface area for a high energy density and interconnected conductive networks for fast charging/discharging processes. CNT sponges, which can be directly synthesized using CVD methods, can be used as additives in Li-ion batteries[167] or solid-state fluoride-ion batteries (e.g., CaF_2, MgF_2).[168] The CNT sponge offers accommodation to buffer the volume change and improves the power density in bio-electrochemical system[169] owing to the continuous 3D conductive path and appropriate pore sizes of the assembly. Nevertheless, CNT-based composites are less competitive than their counterparts, such as graphene-based aerogels and carbon fiber aerogels, because the methods for finely tuning the CNT types (e.g., chirality and wall numbers) in macroaggregates remain limited. The development of CNT-based 3D composites is still in its infancy; therefore, there is considerable room for improvement.

CNT-based 3D assemblies are also promising for catalysis. For example, Figure 8E shows that a high-performing catalyst (Pd) loaded with a CNT sponge[156] exhibited accelerated electrochemical reactivity in Li-air batteries. By simply infiltrating CdS nanoparticles into a CNT sponge, Li et al. prepared a CNT/CdS hybrid for photocatalysis, resulting in the efficient catalytic decomposition of organic dyes.[170] Through a pyrrole-assisted hydrothermal reaction, Du et al. fabricated an N-doped CNT aerogel with high O_2 reduction reaction performance.[171]

In general, the past few decades have witnessed promising breakthroughs in the synthesis and application of CNT macroaggregates. Further expanding their range of applications requires ingenious utilization of the uniqueness and diversity of CNTs, as well as the development of methods to subtly control and modulate their geometric and electronic structures.

PERSPECTIVE

The diversity of the band structures of CNTs endows them with broad application prospects but also challenges. From the development of different CNT devices, we find that CNT-based devices are moving in two directions—they tend to be smaller or larger (Figure 9). To be smaller means that most microelectronic devices, such as FETs, RF devices, and memory devices, need reduced sizes for achieving a high integration density, which is necessary in modern society. The 1D-structured CNTs with a nanoscale diameter and excellent transport properties show great advantages in next-generation nanoelectronic systems. However, the imperfections of the materials used in these devices limit their performances to some degree. In 2013, IBM proposed that for CNT arrays used in transistors, the final approaches for achieving both more than 99.9999% of semiconducting tubes and a CNT density of more than 125 tubes per micrometer with a consistent pitch must be compatible.[39] Among the currently available techniques, direct growth methods give the best purity and orientation but provide relatively low selectivity or low density. Solution separation approaches provide the best selectivity but low orientation, and surfactants remain. Therefore, developing and optimizing the growth technologies to realize controlled synthesis is the key to obtaining better performance of "small" devices. On the other hand, device-manufacture technology also played an important role in promoting the development of CNT microelectronics, such as

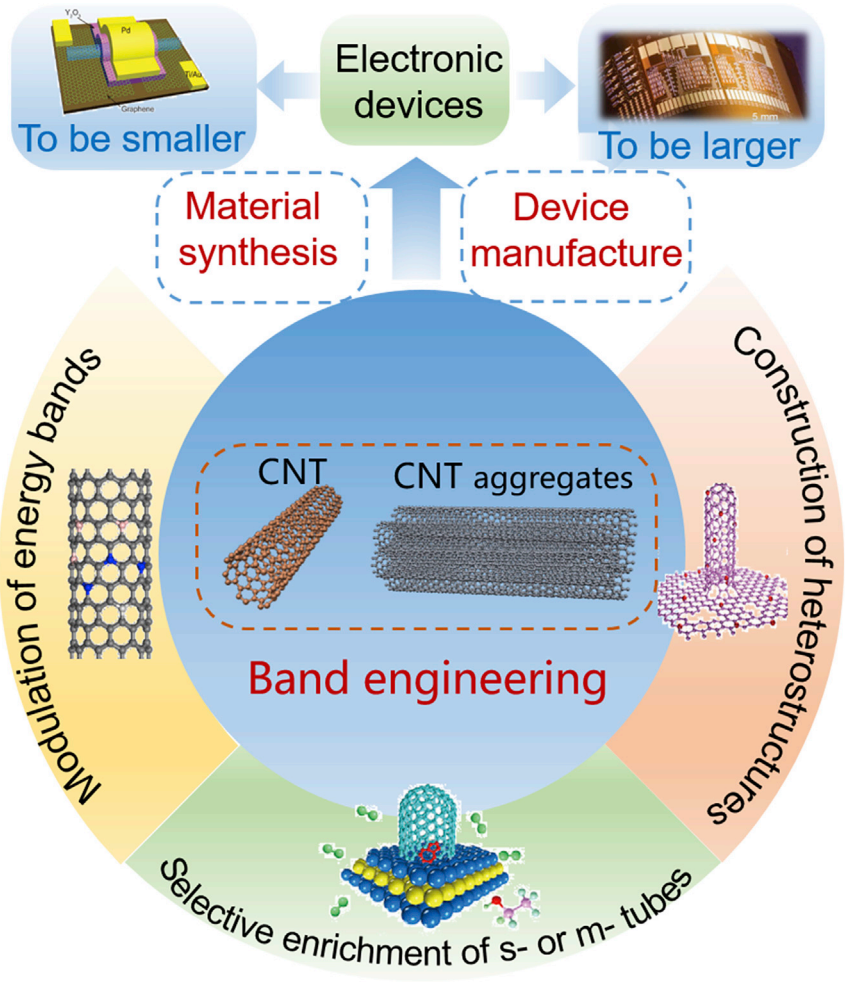

Figure 9. Summary and Perspective for CNT-Based Electronic Devices
From Zhang et al.,[27] Tian et al.,[64] Qiu et al.,[80] and Cao et al.[135] Adapted with permission from Tian et al.[64] Copyright 2014, John Wiley and Sons; Adapted with permission from Zhang et al.[27] Copyright 2019, Elsevier; Adapted with permission from Qiu et al.[80] Copyright 2017,The American Association for the Advancement of Science; Adapted with permission from Cao et al.[135] Copyright 2008, Springer Nature.

optimization of the contact interface and the design of T-shaped gates and floating gates. In the RV16X-NANO system, a special circuit design was used to almost eliminate the influence of metallic CNTs, which enlightened a way to overcome the major intrinsic CNT problems through processing and design techniques. Another promising "small" device of CNTs is the room-temperature single-electron transistor, which requires special processing of a single CNT to introduce local barriers into the tube, such as mechanical buckling,[53] chemical modification,[172] and defect introduction.[173]

For CNT aggregate-based "large" devices, such as TFTs and solar cells, the CNT products are relatively larger and mass production is the basis for practical applications. Therefore, the mass-production technology and the preparation of aggregates are important. CNT powders and aerogels have been obtained through fluid-bed and floating-catalyst CVD. The biggest challenge is controlling the structures or properties of CNTs in mass-production systems. The design of the catalysts

and the introduction of external fields to control the growth process may be effective. The property gap between CNT aggregates and individual CNT is another challenge. In the preparation of CNT aggregates and composites, there are three main factors to be considered: domain size, interactions, and assembly structures. For example, in TCFs, long tubes with ohmic contacts and few overlaps are required.

In both "small" and "large" devices, band engineering of CNTs is worthy of consideration. All the strategies of band engineering are designed to improve the device performance. The selective enrichment of CNTs with a specific electrical property is the material foundation for devices; the modulation of CNT energy bands is helpful in fabricating specific devices, such as N-doping. These two strategies are sometimes necessary in device applications, and efforts should be made to decrease damage to and contamination of CNTs. Moreover, with the increasing number of other emerging nanomaterials, the construction of heterostructures can effectively broaden the application range of CNTs and improve the performances of the hybrids, which is also promising for future applications.

In summary, for commercial applications of CNT-based devices, efforts must be directed toward balancing the cost, performance, and yield. According to the development history of both "small" and "large" devices, the improvement of the comprehensive performance is related to the advancements in the material techniques and the device fabrication techniques (Figure 9), and material preparation may be the key to make further breakthroughs. Controlled synthesis will determine the future applications, and proper manufacture will improve the application qualities. We believe that CNTs, together with suitable band engineering, will finally find their "killer applications" in devices.

ACKNOWLEDGMENTS

This work was supported in part by grants from the Ministry of Science and Technology of the People's Republic of China (2016YFA0200101, 2016YFA0200104 and 2018YFA0703502), the National Natural Science Foundation of China (grant nos. 21790052 and 51720105003), and the China Postdoctoral Science Foundation (grant nos. 8206300206). This work was supported by Beijing National Laboratory for Molecular Sciences (BNLMS- CXTD-202001).

AUTHOR CONTRIBUTIONS

Conceptualization, J.Z., L.Q., and S.Z.; Investigation, L.Q. and Y.X.; Writing – Original Draft, L.Q. and Y.X.; Writing – Review & Editing, L.Q., Y.X., S.Z., and J.Z.; Supervision, J.Z.

REFERENCES

1. Franklin, A.D. (2015). Nanomaterials in transistors: from high-performance to thin-film applications. Science *349*, aab2750.

2. De Volder, M.F.L., Tawfick, S.H., Baughman, R.H., and Hart, A.J. (2013). Carbon nanotubes: present and future commercial applications. Science *339*, 535–539.

3. Shulaker, M.M., Hills, G., Patil, N., Wei, H., Chen, H.-Y., Wong, H.S.P., and Mitra, S. (2013). Carbon nanotube computer. Nature *501*, 526–530.

4. Hills, G., Lau, C., Wright, A., Fuller, S., Bishop, M.D., Srimani, T., Kanhaiya, P., Ho, R., Amer, A., Stein, Y., et al. (2019). Modern microprocessor built from complementary carbon nanotube transistors. Nature *572*, 595–602.

5. Wang, C., Takei, K., Takahashi, T., and Javey, A. (2013). Carbon nanotube electronics—moving forward. Chem. Soc. Rev. *42*, 2592–2609.

6. Zhang, Z.Y., Wang, S., Ding, L., Liang, X.L., Xu, H.L., Shen, J., Chen, Q., Cui, R.L., Li, Y., and Peng, L.-M. (2008). High-performance n-type carbon nanotube field-effect transistors with estimated sub-10-ps gate delay. Appl. Phys. Lett. *92*, 133117.

7. Tune, D.D., and Flavel, B.S. (2018). Advances in carbon nanotube-silicon heterojunction solar cells. Adv. Energy Mater. *8*, 1703241.

8. Charlier, J.-C., Blase, X., and Roche, S. (2007). Electronic and transport properties of nanotubes. Rev. Mod. Phys. *79*, 677–732.

9. Laird, E.A., Kuemmeth, F., Steele, G.A., Grove-Rasmussen, K., Nygård, J., Flensberg, K., and Kouwenhoven, L.P. (2015). Quantum transport in carbon nanotubes. Rev. Mod. Phys. *87*, 703–764.

10. Warner, J.H., Young, N.P., Kirkland, A.I., and Briggs, G.A.D. (2011). Resolving strain in

carbon nanotubes at the atomic level. Nat. Mater. *10*, 958–962.

11. Venema, L.C., Wildöer, J.W.G., Dekker, C., Rinzler, G.A., and Smalley, R.E. (1998). STM atomic resolution images of single-wall carbon nanotubes. Appl. Phys. A *66*, S153–S155.

12. Itkis, M.E., Niyogi, S., Meng, M.E., Hamon, M.A., Hu, H., and Haddon, R.C. (2002). Spectroscopic study of the Fermi level electronic structure of single-walled carbon nanotubes. Nano Lett. *2*, 155–159.

13. Saito, R., Fujita, M., Dresselhaus, G., and Dresselhaus, M.S. (1992). Electronic structure of chiral graphene tubules. Appl. Phys. Lett. *60*, 2204–2206.

14. Hamada, N., Sawada, S.-i., and Oshiyama, A. (1992). New one-dimensional conductors: graphitic microtubules. Phys. Rev. Lett. *68*, 1579–1581.

15. Saito, R., Fujita, M., Dresselhaus, G., and Dresselhaus, M.S. (1992). Electronic structure of graphene tubules based on C_{60}. Phys. Rev. B *46*, 1804–1811.

16. Ouyang, M., Huang, J.-L., Cheung, C.L., and Lieber, C.M. (2001). Energy gaps in "metallic" single-walled carbon nanotubes. Science *292*, 702–705.

17. Blase, X., Benedict, L.X., Shirley, E.L., and Louie, S.G. (1994). Hybridization effects and metallicity in small radius carbon nanotubes. Phys. Rev. Lett. *72*, 1878–1881.

18. Charlier, J.C., and Lambin, P. (1998). Electronic structure of carbon nanotubes with chiral symmetry. Phys. Rev. B *57*, R15037–R15039.

19. Delaney, P., Choi, H.J., Ihm, J., Louie, S.G., and Cohen, M.L. (1998). Broken symmetry and pseudogaps in ropes of carbon nanotubes. Nature *391*, 466–468.

20. Stahl, H., Appenzeller, J., Martel, R., Avouris, P., and Lengeler, B. (2000). Intertube coupling in ropes of single-wall carbon nanotubes. Phys. Rev. Lett. *85*, 5186–5189.

21. Zhang, S., Kang, L., Wang, X., Tong, L., Yang, L., Wang, Z., Qi, K., Deng, S., Li, Q., Bai, X., et al. (2017). Arrays of horizontal carbon nanotubes of controlled chirality grown using designed catalysts. Nature *543*, 234–238.

22. Wang, J., Jin, X., Liu, Z., Yu, G., Ji, Q., Wei, H., Zhang, J., Zhang, K., Li, D., Yuan, Z., et al. (2018). Growing highly pure semiconducting carbon nanotubes by electrotwisting the helicity. Nat. Catal. *1*, 326–331.

23. Zhu, Z., Wei, N., Cheng, W., Shen, B., Sun, S., Gao, J., Wen, Q., Zhang, R., Xu, J., Wang, Y., et al. (2019). Rate-selected growth of ultrapure semiconducting carbon nanotube arrays. Nat. Commun. *10*, 4467.

24. Arnold, M.S., Green, A.A., Hulvat, J.F., Stupp, S.I., and Hersam, M.C. (2006). Sorting carbon nanotubes by electronic structure using density differentiation. Nat. Nanotechnol. *1*, 60–65.

25. Yang, F., Wang, X., Zhang, D.Q., Yang, J., Luo, D., Xu, Z.W., Wei, J.K., Wang, J.Q., Xu, Z., Peng, F., et al. (2014). Chirality-specific growth of single-walled carbon nanotubes on solid alloy catalysts. Nature *510*, 522–524.

26. Zhang, S.C., Hu, Y., Wu, J.X., Liu, D., Kang, L.X., Zhao, Q.C., and Zhang, J. (2015). Selective scission of C-O and C-C bonds in ethanol using bimetal catalysts for the preferential growth of semiconducting SWNT arrays. J. Am. Chem. Soc. *137*, 1012–1015.

27. Zhang, S., Wang, X., Yao, F., He, M., Lin, D., Ma, H., Sun, Y., Zhao, Q., Liu, K., Ding, F., et al. (2019). Controllable growth of (n, n - 1) family of semiconducting carbon nanotubes. Chem *5*, 1182–1193.

28. Kang, L.X., Zhang, S.C., Li, Q.W., and Zhang, J. (2016). Growth of horizontal semiconducting SWNT arrays with density higher than 100 tubes/μm using ethanol/methane chemical vapor deposition. J. Am. Chem. Soc. *138*, 6727–6730.

29. Zhang, G.Y., Qi, P.F., Wang, X.R., Lu, Y.R., Li, X.L., Tu, R., Bangsaruntip, S., Mann, D., Zhang, L., and Dai, H.J. (2006). Selective etching of metallic carbon nanotubes by gas-phase reaction. Science *314*, 974–977.

30. Hong, G., Zhang, B., Peng, B.H., Zhang, J., Choi, W.M., Choi, J.Y., Kim, J.M., and Liu, Z.F. (2009). Direct growth of semiconducting single-walled carbon nanotube array. J. Am. Chem. Soc. *131*, 14642–14643.

31. Jin, S.H., Dunham, S.N., Song, J.Z., Xie, X., Kim, J.H., Lu, C.F., Islam, A., Du, F., Kim, J., Felts, J., et al. (2013). Using nanoscale thermocapillary flows to create arrays of purely semiconducting single-walled carbon nanotubes. Nat. Nanotechnol. *8*, 347–355.

32. Xie, X., Jin, S.H., Wahab, M.A., Islam, A.E., Zhang, C.X., Du, F., Seabron, E., Lu, T.J., Dunham, S.N., Cheong, H.I., et al. (2014). Microwave purification of large-area horizontally aligned arrays of single-walled carbon nanotubes. Nat. Commun. *5*, 5332.

33. Du, F., Felts, J.R., Xie, X., Song, J.Z., Li, Y.H., Rosenberger, M.R., Islam, A.E., Jin, S.H., Dunham, S.N., Zhang, C.X., et al. (2014). Laser-induced nanoscale thermocapillary flow for purification of aligned arrays of single-walled carbon nanotubes. ACS Nano *8*, 12641–12649.

34. Hong, G., Zhou, M., Zhang, R.O.X., Hou, S.M., Choi, W., Woo, Y.S., Choi, J.Y., Liu, Z.F., and Zhang, J. (2011). Separation of metallic and semiconducting single-walled carbon nanotube arrays by "Scotch tape". Angew. Chem. Int. Ed. *50*, 6819–6823.

35. Hu, Y., Chen, Y.B., Li, P., and Zhang, J. (2013). Sorting out semiconducting single-walled carbon nanotube arrays by washing off metallic tubes using SDS aqueous solution. Small *9*, 1306–1311.

36. Liu, H., Nishide, D., Tanaka, T., and Kataura, H. (2011). Large-scale single-chirality separation of single-wall carbon nanotubes by simple gel chromatography. Nat. Commun. *2*, 309.

37. Khripin, C.Y., Fagan, J.A., and Zheng, M. (2013). Spontaneous partition of carbon nanotubes in polymer-modified aqueous phases. J. Am. Chem. Soc. *135*, 6822–6825.

38. Nish, A., Hwang, J.Y., Doig, J., and Nicholas, R.J. (2007). Highly selective dispersion of single-walled carbon nanotubes using aromatic polymers. Nat. Nanotechnol. *2*, 640–646.

39. Franklin, A.D. (2013). The road to carbon nanotube transistors. Nature *498*, 443.

40. Maiti, U.N., Lee, W.J., Lee, J.M., Oh, Y., Kim, J.Y., Kim, J.E., Shim, J., Han, T.H., and Kim, S.O. (2014). 25th anniversary article: chemically modified/doped carbon nanotubes & graphene for optimized nanostructures & nanodevices. Adv. Mater. *26*, 40–67.

41. Czerw, R., Terrones, M., Charlier, J.C., Blase, X., Foley, B., Kamalakaran, R., Grobert, N., Terrones, H., Tekleab, D., Ajayan, P.M., et al. (2001). Identification of electron donor states in N-doped carbon nanotubes. Nano Lett. *1*, 457–460.

42. Sumpter, B.G., Meunier, V., Romo-Herrera, J.M., Cruz-Silva, E., Cullen, D.A., Terrones, H., Smith, D.J., and Terrones, M. (2007). Nitrogen-mediated carbon nanotube growth: diameter reduction, metallicity, bundle dispersability, and bamboo-like structure formation. ACS Nano *1*, 369–375.

43. Gebhardt, J., Koch, R.J., Zhao, W., Höfert, O., Gotterbarm, K., Mammadov, S., Papp, C., Görling, A., Steinrück, H.P., and Seyller, T. (2013). Growth and electronic structure of boron-doped graphene. Phys. Rev. B *87*, 155437.

44. Carroll, D.L., Redlich, P., Blase, X., Charlier, J.C., Curran, S., Ajayan, P.M., Roth, S., and Ruhle, M. (1998). Effects of nanodomain formation on the electronic structure of doped carbon nanotubes. Phys. Rev. Lett. *81*, 2332–2335.

45. Kim, K.K., Bae, J.J., Park, H.K., Kim, S.M., Geng, H.Z., Park, K.A., Shin, H.J., Yoon, S.M., Benayad, A., Choi, J.Y., et al. (2008). Fermi level engineering of single-walled carbon nanotubes by $AuCl_3$ doping. J. Am. Chem. Soc. *130*, 12757–12761.

46. Li, Y., Rotkin, S.V., and Ravaioli, U. (2003). Electronic response and bandstructure modulation of carbon nanotubes in a transverse electrical field. Nano Lett. *3*, 183–187.

47. Chen, C.-W., Lee, M.-H., and Clark, S.J. (2004). Band gap modification of single-walled carbon nanotube and boron nitride nanotube under a transverse electric field. Nanotechnology *15*, 1837–1843.

48. Kim, Y.-H., and Chang, K.J. (2001). Subband mixing rules in circumferentially perturbed carbon nanotubes: effects of transverse electric fields. Phys. Rev. B *64*, 153404.

49. Gülseren, O., Yildirim, T., Ciraci, S., and Kılıç, Ç. (2002). Reversible band-gap engineering in carbon nanotubes by radial deformation. Phys. Rev. B *65*, 155410.

50. Wang, Z., Zhou, Y., Zhang, Y., and Gao, F. (2012). Band-gap engineering of carbon nanotubes with grain boundaries. J. Phys. Chem. C *116*, 2271–2277.

51. Yao, Z., Postma, H.W.C., Balents, L., and Dekker, C. (1999). Carbon nanotube

intramolecular junctions. Nature *402*, 273–276.

52. Chen, C., Song, C., Yang, J., Chen, D., Zhu, W., Liao, C., Dong, X., Liu, X., Wei, L., and Hu, N. (2017). Intramolecular pin junction photovoltaic device based on selectively doped carbon nanotubes. Nano Energy *32*, 280–286.

53. Postma, H.W.C., Teepen, T., Yao, Z., Grifoni, M., and Dekker, C. (2001). Carbon nanotube single-electron transistors at room temperature. Science *293*, 76.

54. Yao, Y., Li, Q., Zhang, J., Liu, R., Jiao, L., Zhu, Y.T., and Liu, Z. (2007). Temperature-mediated growth of single-walled carbon-nanotube intramolecular junctions. Nat. Mater. *6*, 283–286.

55. Jin, C., Suenaga, K., and Iijima, S. (2008). Plumbing carbon nanotubes. Nat. Nanotech. *3*, 17.

56. Dissanayake, N.M., and Zhong, Z. (2011). Unexpected hole transfer leads to high efficiency single-walled carbon nanotube hybrid photovoltaic. Nano Lett. *11*, 286–290.

57. Eder, D. (2010). Carbon nanotube-inorganic hybrids. Chem. Rev. *110*, 1348–1385.

58. Freeley, M., Attanzio, A., Cecconello, A., Amoroso, G., Clement, P., Fernandez, G., Gesuele, F., and Palma, M. (2018). Tuning the coupling in single-molecule heterostructures: DNA-programmed and reconfigurable carbon nanotube-based nanohybrids. Adv. Sci. *5*, 1800596.

59. Xiang, R., Inoue, T., Zheng, Y., Kumamoto, A., Qian, Y., Sato, Y., Liu, M., Tang, D., Gokhale, D., Guo, J., et al. (2020). One-dimensional van der Waals heterostructures. Science *367*, 537.

60. Cook, B.G., French, W.R., and Varga, K. (2012). Electron transport properties of carbon nanotube-graphene contacts. Appl. Phys. Lett. *101*, 153501.

61. Zhang, J., Zhang, K., Xia, B., Wei, Y., Li, D., Zhang, K., Zhang, Z., Wu, Y., Liu, P., Duan, X., et al. (2017). Carbon-nanotube-confined vertical heterostructures with asymmetric contacts. Adv. Mater. *29*, 1702942.

62. Mieszawska, A.J., Jalilian, R., Sumanasekera, G.U., and Zamborini, F.P. (2005). Synthesis of gold nanorod/single-wall carbon nanotube heterojunctions directly on surfaces. J. Am. Chem. Soc. *127*, 10822–10823.

63. Sandoval, S., Kepić, D., Pérez del Pino, Á., György, E., Gómez, A., Pfannmoeller, M., Tendeloo, G.V., Ballesteros, B., and Tobias, G. (2018). Selective laser-assisted synthesis of tubular van der Waals heterostructures of single-layered PbI_2 within carbon nanotubes exhibiting carrier photogeneration. ACS Nano *12*, 6648–6656.

64. Tian, G.-L., Zhao, M.-Q., Yu, D., Kong, X.-Y., Huang, J.-Q., Zhang, Q., and Wei, F. (2014). Nitrogen-doped graphene/carbon nanotube hybrids: in situ formation on bifunctional catalysts and their superior electrocatalytic activity for oxygen evolution/reduction reaction. Small *10*, 2251–2259.

65. Mao, Y., and Zhong, J. (2009). The computational design of junctions by carbon nanotube insertion into a graphene matrix. New J. Phys. *11*, 093002.

66. Artyukh, A.A., Chernozatonskii, L.A., and Sorokin, P.B. (2010). Mechanical and electronic properties of carbon nanotube-graphene compounds. Phys. Status Solidi B *247*, 2927–2930.

67. Gangavarapu, P.R.Y., Lokesh, P.C., Bhat, K.N., and Naik, A.K. (2017). Graphene electrodes as barrier-free contacts for carbon nanotube field-effect transistors. IEEE Trans. Electron Devices *64*, 4335–4339.

68. Nguyen, V.T., Yim, W., Park, S.J., Son, B.H., Kim, Y.C., Cao, T.T., Sim, Y., Moon, Y.-J., Nguyen, V.C., Seong, M.-J., et al. (2018). Phototransistors with negative or ambipolar photoresponse based on as-grown heterostructures of single-walled carbon nanotube and MoS_2. Adv. Funct. Mater. *28*, 1802572.

69. Adams, G.R., Adhikari, N., Parker, H., and Okoli, O. (2018). Flexible wire-shaped perovskite photodetector via Joule heating for improved crystallization and performance. Adv. Mater. Interfaces *5*, 1800082.

70. Wang, W., and Kumta, P.N. (2010). Nanostructured hybrid silicon/carbon nanotube heterostructures: reversible high-capacity lithium-ion anodes. ACS Nano *4*, 2233–2241.

71. Tans, S.J., Verschueren, A.R.M., and Dekker, C. (1998). Room-temperature transistor based on a single carbon nanotube. Nature *393*, 49–52.

72. Javey, A., Kim, H., Brink, M., Wang, Q., Ural, A., Guo, J., McIntyre, P., McEuen, P., Lundstrom, M., and Dai, H. (2002). High-κ dielectrics for advanced carbon-nanotube transistors and logic gates. Nat. Mater. *1*, 241–246.

73. Javey, A., Guo, J., Farmer, D.B., Wang, Q., Wang, D., Gordon, R.G., Lundstrom, M., and Dai, H. (2004). Carbon nanotube field-effect transistors with integrated ohmic contacts and high-κ gate dielectrics. Nano Lett. *4*, 447–450.

74. Wang, Z., Xu, H., Zhang, Z., Wang, S., Ding, L., Zeng, Q., Yang, L., Pei, T., Liang, X., Gao, M., et al. (2010). Growth and performance of yttrium oxide as an ideal high-κ gate dielectric for carbon-based electronics. Nano Lett. *10*, 2024–2030.

75. Javey, A., Guo, J., Wang, Q., Lundstrom, M., and Dai, H. (2003). Ballistic carbon nanotube field-effect transistors. Nature *424*, 654–657.

76. Zhang, Z., Wang, S., Ding, L., Liang, X., Pei, T., Shen, J., Xu, H., Chen, Q., Cui, R., Li, Y., et al. (2008). Self-aligned ballistic n-type single-walled carbon nanotube field-effect transistors with adjustable threshold voltage. Nano Lett. *8*, 3696–3701.

77. Franklin, A.D., and Chen, Z. (2010). Length scaling of carbon nanotube transistors. Nat. Nanotechnol. *5*, 858–862.

78. Franklin, A.D., Luisier, M., Han, S.-J., Tulevski, G., Breslin, C.M., Gignac, L., Lundstrom, M.S., and Haensch, W. (2012). Sub-10 nm carbon nanotube transistor. Nano Lett. *12*, 758–762.

79. Cao, Q., Han, S.-J., Tersoff, J., Franklin, A.D., Zhu, Y., Zhang, Z., Tulevski, G.S., Tang, J., and Haensch, W. (2015). End-bonded contacts for carbon nanotube transistors with low, size-independent resistance. Science *350*, 68–72.

80. Qiu, C., Zhang, Z., Xiao, M., Yang, Y., Zhong, D., and Peng, L.-M. (2017). Scaling carbon nanotube complementary transistors to 5-nm gate lengths. Science *355*, 271–276.

81. Bachtold, A., Hadley, P., Nakanishi, T., and Dekker, C. (2001). Logic circuits with carbon nanotube transistors. Science *294*, 1317.

82. Heinze, S., Tersoff, J., Martel, R., Derycke, V., Appenzeller, J., and Avouris, P. (2002). Carbon nanotubes as Schottky barrier transistors. Phys. Rev. Lett. *89*, 106801.

83. Appenzeller, J., Knoch, J., Derycke, V., Martel, R., Wind, S., and Avouris, P. (2002). Field-modulated carrier transport in carbon nanotube transistors. Phys. Rev. Lett. *89*, 126801.

84. Ding, L., Wang, S., Zhang, Z., Zeng, Q., Wang, Z., Pei, T., Yang, L., Liang, X., Shen, J., Chen, Q., et al. (2009). Y-contacted high-performance n-type single-walled carbon nanotube field-effect transistors: scaling and comparison with Sc-contacted devices. Nano Lett. *9*, 4209–4214.

85. Qiu, C., Liu, F., Xu, L., Deng, B., Xiao, M., Si, J., Lin, L., Zhang, Z., Wang, J., Guo, H., et al. (2018). Dirac-source field-effect transistors as energy-efficient, high-performance electronic switches. Science *361*, 387–391.

86. Martel, R. (2002). High-performance transistors. Nat. Mater. *1*, 203–204.

87. Chen, Z., Appenzeller, J., Lin, Y.-M., Sippel-Oakley, J., Rinzler, A.G., Tang, J., Wind, S.J., Solomon, P.M., and Avouris, P. (2006). An integrated logic circuit assembled on a single carbon nanotube. Science *311*, 1735.

88. Chen, B., Zhang, P., Ding, L., Han, J., Qiu, S., Li, Q., Zhang, Z., and Peng, L.-M. (2016). Highly uniform carbon nanotube field-effect transistors and medium scale integrated circuits. Nano Lett. *16*, 5120–5128.

89. Han, S.-J., Tang, J., Kumar, B., Falk, A., Farmer, D., Tulevski, G., Jenkins, K., Afzali, A., Oida, S., Ott, J., et al. (2017). High-speed logic integrated circuits with solution-processed self-assembled carbon nanotubes. Nat. Nanotechnol. *12*, 861–865.

90. Tulevski, G.S., Franklin, A.D., Frank, D., Lobez, J.M., Cao, Q., Park, H., Afzali, A., Han, S.-J., Hannon, J.B., and Haensch, W. (2014). Toward high-performance digital logic technology with carbon nanotubes. ACS Nano *8*, 8730–8745.

91. Liu, L., Han, J., Xu, L., Zhou, J., Zhao, C., Ding, S., Shi, H., Xiao, M., Ding, L., Ma, Z., et al. (2020). Aligned, high-density semiconducting carbon nanotube arrays for high-performance electronics. Science *368*, 850–856.

92. Zhao, M., Chen, Y., Wang, K., Zhang, Z., Streit, J.K., Fagan, J.A., Tang, J., Zheng, M., Yang, C., Zhu, Z., et al. (2020). DNA-directed nanofabrication of high-performance carbon nanotube field-effect transistors. Science *368*, 878–881.

93. Sun, W., Shen, J., Zhao, Z., Arellano, N., Rettner, C., Tang, J., Cao, T., Zhou, Z., Ta, T., Streit, J.K., et al. (2020). Precise pitch-scaling of carbon nanotube arrays within three-dimensional DNA nanotrenches. Science *368*, 874–877.

94. Maas, S.. (2017).Linearity and dynamic range of carbon nanotube field-effect transistors. IEEE MTT-S International Microwave Symposium (IMS), pp. 87-90.10.1109/MWSYM.2017.8058727

95. Jensen, K., Weldon, J., Garcia, H., and Zettl, A. (2008). Nanotube radio. Nano Lett. *8*, 374.

96. Che, Y., Lin, Y.-C., Kim, P., and Zhou, C. (2013). T-gate aligned nanotube radio frequency transistors and circuits with superior performance. ACS Nano *7*, 4343–4350.

97. Rutherglen, C., Kane, A.A., Marsh, P.F., Cain, T.A., Hassan, B.I., AlShareef, M.R., Zhou, C., and Galatsis, K. (2019). Wafer-scalable, aligned carbon nanotube transistors operating at frequencies of over 100 GHz. Nat. Electron. *2*, 530–539.

98. Qu, T.-Y., Sun, Y., Chen, M.-L., Liu, Z.-B., Zhu, Q.-B., Wang, B.-W., Zhao, T.-Y., Liu, C., Tan, J., Qiu, S., et al. (2020). A flexible carbon nanotube Sen-memory device. Adv. Mater. *32*, 1907288.

99. He, X., Fujimura, N., Lloyd, J.M., Erickson, K.J., Talin, A.A., Zhang, Q., Gao, W., Jiang, Q., Kawano, Y., Hauge, R.H., et al. (2014). Carbon nanotube terahertz detector. Nano Lett. *14*, 3953–3958.

100. Graf, A., Held, M., Zakharko, Y., Tropf, L., Gather, M.C., and Zaumseil, J. (2017). Electrical pumping and tuning of exciton-polaritons in carbon nanotube microcavities. Nat. Mater. *16*, 911–917.

101. Salehi-Khojin, A., Khalili-Araghi, F., Kuroda, M.A., Lin, K.Y., Leburton, J.-P., and Masel, R.I. (2011). On the sensing mechanism in carbon nanotube chemiresistors. ACS Nano *5*, 153–158.

102. Li, F., Wang, H., Kufer, D., Liang, L., Yu, W., Alarousu, E., Ma, C., Li, Y., Liu, Z., Liu, C., et al. (2017). Ultrahigh carrier mobility achieved in photoresponsive hybrid perovskite films via coupling with single-walled carbon nanotubes. Adv. Mater. *29*, 1602432.

103. Lu, G., Ocola, L.E., and Chen, J. (2009). Room-temperature gas sensing based on electron transfer between discrete tin oxide nanocrystals and multiwalled carbon nanotubes. Adv. Mater. *21*, 2487–2491.

104. Radosavljević, M., Freitag, M., Thadani, K.V., and Johnson, A.T. (2002). Nonvolatile molecular memory elements based on ambipolar nanotube field effect transistors. Nano Lett. *2*, 761–764.

105. Chido, M.T., Koronaios, P., Saravanan, K., Adams, A.P., Geib, S.J., Zhu, Q., Sunkara, H.B., Velankar, S.S., Enick, R.M., Keith, J.A., et al. (2018). Oligomer hydrate crystallization improves carbon nanotube memory. Chem. Mater. *30*, 3813–3818.

106. Nanot, S., Hároz, E.H., Kim, J.-H., Hauge, R.H., and Kono, J. (2012). Optoelectronic properties of single-wall carbon nanotubes. Adv. Mater. *24*, 4977–4994.

107. Barkelid, M., and Zwiller, V. (2014). Photocurrent generation in semiconducting and metallic carbon nanotubes. Nat. Photon. *8*, 47–51.

108. Itkis, M.E., Borondics, F., Yu, A., and Haddon, R.C. (2006). Bolometric infrared photoresponse of suspended single-walled carbon nanotube films. Science *312*, 413–416.

109. Yang, L., Wang, S., Zeng, Q., Zhang, Z., Pei, T., Li, Y., and Peng, L.-M. (2011). Efficient photovoltage multiplication in carbon nanotubes. Nat. Photon. *5*, 672–676.

110. Liu, Y., Wei, N., Zhao, Q., Zhang, D., Wang, S., and Peng, L.-M. (2015). Room temperature infrared imaging sensors based on highly purified semiconducting carbon nanotubes. Nanoscale *7*, 6805–6812.

111. Liu, Y., Wei, N., Zeng, Q., Han, J., Huang, H., Zhong, D., Wang, F., Ding, L., Xia, J., Xu, H., et al. (2016). Room temperature broadband infrared carbon nanotube photodetector with high detectivity and stability. Adv.Opt. Mater. *4*, 238–245.

112. Zhang, L., Wu, Y., Deng, L., Zhou, Y., Liu, C., and Fan, S. (2016). Photodetection and photoswitch based on polarized optical response of macroscopically aligned carbon nanotubes. Nano Lett. *16*, 6378–6382.

113. Zhang, S., Cai, L., Wang, T., Miao, J., Sepúlveda, N., and Wang, C. (2017). Fully printed flexible carbon nanotube photodetectors. Appl. Phys. Lett. *110*, 123105.

114. Zubair, A., Wang, X., Mirri, F., Tsentalovich, D.E., Fujimura, N., Suzuki, D., Soundarapandian, K.P., Kawano, Y., Pasquali, M., and Kono, J. (2018). Carbon nanotube woven textile photodetector. Phys. Rev. Mater. *2*, 015201.

115. Freitag, M., Chen, J., Tersoff, J., Tsang, J.C., Fu, Q., Liu, J., and Avouris, P. (2004). Mobile ambipolar domain in carbon-nanotube infrared emitters. Phys. Rev. Lett. *93*, 076803.

116. Mueller, T., Kinoshita, M., Steiner, M., Perebeinos, V., Bol, A.A., Farmer, D.B., and Avouris, P. (2010). Efficient narrow-band light emission from a single carbon nanotube p-n diode. Nat. Nanotechnol. *5*, 27–31.

117. He, X., Hartmann, N.F., Ma, X., Kim, Y., Ihly, R., Blackburn, J.L., Gao, W., Kono, J., Yomogida, Y., Hirano, A., et al. (2017). Tunable room-temperature single-photon emission at telecom wavelengths from sp3 defects in carbon nanotubes. Nat. Photon. *11*, 577–582.

118. Soylemez, S., Yoon, B., Toppare, L., and Swager, T.M. (2017). Quaternized polymer-single-walled carbon nanotube scaffolds for a chemiresistive glucose sensor. ACS Sensors *2*, 1123–1127.

119. Kong, J., Franklin, N.R., Zhou, C., Chapline, M.G., Peng, S., Cho, K., and Dai, H. (2000). Nanotube molecular wires as chemical sensors. Science *287*, 622–625.

120. Ishihara, S., O'Kelly, C.J., Tanaka, T., Kataura, H., Labuta, J., Shingaya, Y., Nakayama, T., Ohsawa, T., Nakanishi, T., and Swager, T.M. (2017). Metallic versus semiconducting SWCNT chemiresistors: a case for separated SWCNTs wrapped by a metallosupramolecular polymer. ACS Appl. Mater. Interfaces *9*, 38062–38067.

121. Schroeder, V., Savagatrup, S., He, M., Lin, S., and Swager, T.M. (2019). Carbon nanotube chemical sensors. Chem. Rev. *119*, 599–663.

122. Ding, M., Sorescu, D.C., and Star, A. (2013). Photoinduced charge transfer and acetone sensitivity of single-walled carbon nanotube-titanium dioxide hybrids. J. Am. Chem. Soc. *135*, 9015–9022.

123. Heller, D.A., Baik, S., Eurell, T.E., and Strano, M.S. (2005). Single-walled carbon nanotube spectroscopy in live cells: towards long-term labels and optical sensors. Adv. Mater. *17*, 2793–2799.

124. Jariwala, D., Sangwan, V.K., Wu, C.-C., Prabhumirashi, P.L., Geier, M.L., Marks, T.J., Lauhon, L.J., and Hersam, M.C. (2013). Gate-tunable carbon nanotube-MoS_2 heterojunction p-n diode. Proc. Natl. Acad. Sci. U S A *110*, 18076.

125. Liu, Y., Wang, F., Wang, X., Wang, X., Flahaut, E., Liu, X., Li, Y., Wang, X., Xu, Y., Shi, Y., et al. (2015). Planar carbon nanotube-graphene hybrid films for high-performance broadband photodetectors. Nat. Commun. *6*, 8589.

126. Liu, Y., Liu, Y., Qin, S., Xu, Y., Zhang, R., and Wang, F. (2017). Graphene-carbon nanotube hybrid films for high-performance flexible photodetectors. Nano Res. *10*, 1880–1887.

127. Park, S., Kim, S.J., Nam, J.H., Pitner, G., Lee, T.H., Ayzner, A.L., Wang, H., Fong, S.W., Vosgueritchian, M., Park, Y.J., et al. (2015). Significant enhancement of infrared photodetector sensitivity using a semiconducting single-walled carbon nanotube/C_{60} phototransistor. Adv. Mater. *27*, 759–765.

128. Kong, J., Chapline, M.G., and Dai, H. (2001). Functionalized carbon nanotubes for molecular hydrogen sensors. Adv. Mater. *13*, 1384–1386.

129. Sun, D.-m., Timmermans, M.Y., Tian, Y., Nasibulin, A.G., Kauppinen, E.I., Kishimoto, S., Mizutani, T., and Ohno, Y. (2011). Flexible high-performance carbon nanotube integrated circuits. Nat. Nanotechnol. *6*, 156–161.

130. Wang, B.-W., Jiang, S., Zhu, Q.-B., Sun, Y., Luan, J., Hou, P.-X., Qiu, S., Li, Q.-W., Liu, C., Sun, D.-M., et al. (2018). Continuous fabrication of meter-scale single-wall carbon nanotube films and their use in flexible and transparent integrated circuits. Adv. Mater. *30*, 1802057.

131. Thanh, Q.N., Jeong, H., Kim, J., Kevek, J.W., Ahn, Y.H., Lee, S., Minot, E.D., and Park, J.-Y. (2012). Transfer-printing of As-fabricated carbon nanotube devices onto various substrates. Adv. Mater. *24*, 4499–4504.

132. Okimoto, H., Takenobu, T., Yanagi, K., Miyata, Y., Shimotani, H., Kataura, H., and Iwasa, Y. (2010). Tunable carbon nanotube thin-film transistors produced exclusively via inkjet printing. Adv. Mater. *22*, 3981–3986.

133. Tang, J., Cao, Q., Tulevski, G., Jenkins, K.A., Nela, L., Farmer, D.B., and Han, S.-J. (2018). Flexible CMOS integrated circuits based on

carbon nanotubes with sub-10 ns stage delays. Nat. Electron. *1*, 191–196.

134. Feng, C., Liu, K., Wu, J.-S., Liu, L., Cheng, J.-S., Zhang, Y., Sun, Y., Li, Q., Fan, S., and Jiang, K. (2010). Flexible, stretchable, transparent conducting films made from superaligned carbon nanotubes. Adv. Funct. Mater. *20*, 885–891.

135. Cao, Q., Kim, H.-s., Pimparkar, N., Kulkarni, J.P., Wang, C., Shim, M., Roy, K., Alam, M.A., and Rogers, J.A. (2008). Medium-scale carbon nanotube thin-film integrated circuits on flexible plastic substrates. Nature *454*, 495–500.

136. Lau, P.H., Takei, K., Wang, C., Ju, Y., Kim, J., Yu, Z., Takahashi, T., Cho, G., and Javey, A. (2013). Fully printed, high performance carbon nanotube thin-film transistors on flexible substrates. Nano Lett. *13*, 3864–3869.

137. Zhang, L., Sun, D.-M., Hou, P.-X., Liu, C., Liu, T., Wen, J., Tang, N., Luan, J., Shi, C., Li, J.-C., et al. (2017). Selective growth of metal-free metallic and semiconducting single-wall carbon nanotubes. Adv. Mater. *29*, 1605719.

138. Zhu, M.-G., Si, J., Zhang, Z., and Peng, L.-M. (2018). Aligning solution-derived carbon nanotube film with full surface coverage for high-performance electronics applications. Adv. Mater. *30*, 1707068.

139. Mirri, F., Ma, A.W.K., Hsu, T.T., Behabtu, N., Eichmann, S.L., Young, C.C., Tsentalovich, D.E., and Pasquali, M. (2012). High-performance carbon nanotube transparent conductive films by scalable dip coating. ACS Nano *6*, 9737–9744.

140. Jiang, S., Hou, P.-X., Chen, M.-L., Wang, B.-W., Sun, D.-M., Tang, D.-M., Jin, Q., Guo, Q.-X., Zhang, D.-D., Du, J.-H., et al. (2018). Ultrahigh-performance transparent conductive films of carbon-welded isolated single-wall carbon nanotubes. Sci. Adv. *4*, eaap9264.

141. Yu, L., Shearer, C., and Shapter, J. (2016). Recent development of carbon nanotube transparent conductive films. Chem. Rev. *116*, 13413–13453.

142. Lee, S.-H., Teng, C.-C., Ma, C.-C.M., and Wang, I. (2011). Highly transparent and conductive thin films fabricated with nano-silver/double-walled carbon nanotube composites. J. Colloid Interface Sci. *364*, 1–9.

143. De, S., Lyons, P.E., Sorel, S., Doherty, E.M., King, P.J., Blau, W.J., Nirmalraj, P.N., Boland, J.J., Scardaci, V., Joimel, J., et al. (2009). Transparent, flexible, and highly conductive thin films based on polymer−nanotube composites. ACS Nano *3*, 714–720.

144. Kurzepa, L., Lekawa-Raus, A., Patmore, J., and Koziol, K. (2014). Replacing copper wires with carbon nanotube wires in electrical transformers. Adv. Funct. Mater. *24*, 619–624.

145. Ma, W., Liu, L., Yang, R., Zhang, T., Zhang, Z., Song, L., Ren, Y., Shen, J., Niu, Z., Zhou, W., et al. (2009). Monitoring a micromechanical process in macroscale carbon nanotube films and fibers. Adv. Mater. *21*, 603–608.

146. Janas, D., Herman, A.P., Boncel, S., and Koziol, K.K.K. (2014). Iodine monochloride as a powerful enhancer of electrical conductivity of carbon nanotube wires. Carbon *73*, 225–233.

147. Zhao, Y., Wei, J., Vajtai, R., Ajayan, P.M., and Barrera, E.V. (2011). Iodine doped carbon nanotube cables exceeding specific electrical conductivity of metals. Sci. Rep. *1*, 83.

148. Beyerlein, I.J., Porwal, P.K., Zhu, Y.T., Hu, K., and Xu, X.F. (2009). Scale and twist effects on the strength of nanostructured yarns and reinforced composites. Nanotechnology *20*, 485702.

149. Sundaram, R.M., Koziol, K.K., and Windle, A.H. (2011). Continuous direct spinning of fibers of single-walled carbon nanotubes with metallic chirality. Adv. Mater. *23*, 5064–5068.

150. Ren, J., Li, L., Chen, C., Chen, X., Cai, Z., Qiu, L., Wang, Y., Zhu, X., and Peng, H. (2013). Twisting carbon nanotube fibers for both wire-shaped micro-supercapacitor and micro-battery. Adv. Mater. *25*, 1155–1159.

151. Dalton, A.B., Collins, S., Munoz, E., Razal, J.M., Ebron, V.H., Ferraris, J.P., Coleman, J.N., Kim, B.G., and Baughman, R.H. (2003). Super-tough carbon-nanotube fibres. Nature *423*, 703.

152. Baughman, R.H., Cui, C., Zakhidov, A.A., Iqbal, Z., Barisci, J.N., Spinks, G.M., Wallace, G.G., Mazzoldi, A., De Rossi, D., Rinzler, A.G., et al. (1999). Carbon nanotube actuators. Science *284*, 1340–1344.

153. Zou, J., Liu, J., Karakoti, A.S., Kumar, A., Joung, D., Li, Q., Khondaker, S.I., Seal, S., and Zhai, L. (2010). Ultralight multiwalled carbon nanotube aerogel. ACS Nano *4*, 7293–7302.

154. Ihly, R., Dowgiallo, A.-M., Yang, M., Schulz, P., Stanton, N.J., Reid, O.G., Ferguson, A.J., Zhu, K., Berry, J.J., and Blackburn, J.L. (2016). Efficient charge extraction and slow recombination in organic-inorganic perovskites capped with semiconducting single-walled carbon nanotubes. Energy Environ. Sci. *9*, 1439–1449.

155. Jin, Q., Jiang, S., Zhao, Y., Wang, D., Qiu, J., Tang, D.M., Tan, J., Sun, D.M., Hou, P.X., Chen, X.Q., et al. (2019). Flexible layer-structured Bi_2Te_3 thermoelectric on a carbon nanotube scaffold. Nat. Mater. *18*, 62–68.

156. Shen, Y., Sun, D., Yu, L., Zhang, W., Shang, Y., Tang, H., Wu, J., Cao, A., and Huang, Y. (2013). A high-capacity lithium-air battery with Pd modified carbon nanotube sponge cathode working in regular air. Carbon *62*, 288–295.

157. Davis, V.L., Quaranta, S., Cavallo, C., Latini, A., and Gaspari, F. (2017). Effect of single-chirality single-walled carbon nanotubes in dye sensitized solar cells photoanodes. Sol. Energy Mater. Sol. Cells *167*, 162–172.

158. Pfohl, M., Glaser, K., Graf, A., Mertens, A., and Flavel, B.S. (2016). Probing the diameter limit of single walled carbon nanotubes in SWCNT: fullerene solar cells. Adv. Energy Mater. *6*, 1600890.

159. Hu, X.-G., Hou, P.-X., Wu, J.-B., Li, X., Luan, J., Liu, C., Liu, G., and Cheng, H.-M. (2020). High-efficiency and stable silicon heterojunction solar cells with lightly fluorinated single-wall carbon nanotube films. Nano Energy *69*, 104442.

160. Tune, D.D., Mallik, N., Fornasier, H., and Flavel, B.S. (2020). Breakthrough carbon nanotube-silicon heterojunction solar cells. Adv. Energy Mater. *10*, 1903261.

161. Cho, C., Wallace, K.L., Tzeng, P., Hsu, J.H., Yu, C., and Grunlan, J.C. (2016). Outstanding low temperature thermoelectric power factor from completely organic thin films enabled by multidimensional conjugated nanomaterials. Adv. Energy Mater. *6*, 1502168.

162. Zhang, M., Zhao, M., Jian, M., Wang, C., Yu, A., Yin, Z., Liang, X., Wang, H., Xia, K., Liang, X., et al. (2019). Printable smart pattern for multifunctional energy-management E-textile. Matter *1*, 168–179.

163. Wang, Q., Wang, C., Zhang, M., Jian, M., and Zhang, Y. (2016). Feeding single-walled carbon nanotubes or graphene to silkworms for reinforced silk fibers. Nano Lett. *16*, 6695–6700.

164. Wang, H., Li, S., Wang, Y., Wang, H., Shen, X., Zhang, M., Lu, H., He, M., and Zhang, Y. (2020). Bioinspired fluffy fabric with in situ grown carbon nanotubes for ultrasensitive wearable airflow sensor. Adv. Mater. *32*, 1908214.

165. Bryning, M.B., Milkie, D.E., Islam, M.F., Hough, L.A., Kikkawa, J.M., and Yodh, A.G. (2007). Carbon nanotube aerogels. Adv. Mater. *19*, 661–664.

166. Wang, W., Guo, S., Penchev, M., Ruiz, I., Bozhilov, K.N., Yan, D., Ozkan, M., and Ozkan, C.S. (2013). Three dimensional few layer graphene and carbon nanotube foam architectures for high fidelity supercapacitors. Nano Energy *2*, 294–303.

167. Hu, L., Wu, H., Gao, Y., Cao, A., Li, H., McDough, J., Xie, X., Zhou, M., and Cui, Y. (2011). Silicon-carbon nanotube coaxial sponge as Li-ion anodes with high areal capacity. Adv. Energy Mater. *1*, 523–527.

168. Zhang, L., Reddy, M.A., and Fichtner, M. (2017). Electrochemical performance of all solid-state fluoride-ion batteries based on thin-film electrolyte using alternative conductive additives and anodes. J. Solid State Electrochem. *22*, 997–1006.

169. Xie, X., Ye, M., Hu, L., Liu, N., McDonough, J.R., Chen, W., Alshareef, H.N., Criddle, C.S., and Cui, Y. (2012). Carbon nanotube-coated macroporous sponge for microbial fuel cell electrodes. Energy Environ. Sci. *5*, 5265–5270.

170. Li, H., Gui, X., Ji, C., Li, P., Li, Z., Zhang, L., Shi, E., Zhu, K., Wei, J., Wang, K., et al. (2012). Photocatalytic, recyclable CdS nanoparticle-carbon nanotube hybrid sponges. Nano Res. *5*, 265–271.

171. Du, R., Zhang, N., Zhu, J., Wang, Y., Xu, C., Hu, Y., Mao, N., Xu, H., Duan, W., Zhuang, L., et al. (2015). Nitrogen-doped carbon nanotube aerogels for high-performance ORR catalysts. Small *11*, 3903–3908.

172. Cui, J.B., Burghard, M., and Kern, K. (2002). Room temperature single electron transistor by local chemical modification of carbon nanotubes. Nano Lett. *2*, 117–120.

173. Maeda, M., Iwasaki, S., Kamimura, T., Murata, K., and Matsumoto, K. (2008). Room-temperature carbon nanotube single-electron transistor with defects introduced by $La(NO_3)_3$ process. Jpn. J. Appl. Phys. *47*, 5724–5726.